

**1 New age constraints reveal moraine stabilization thousands of  
2 years after deposition during the last deglaciation of western  
3 New York, USA**

4

5 Karlee K. Prince<sup>1</sup>, Jason P. Briner<sup>1</sup>, Caleb K. Walcott<sup>1</sup>, Brooke M. Chase<sup>1</sup>, Andrew L.  
6 Kozłowski<sup>2</sup>, Tammy M. Rittenour<sup>3</sup>, Erica P. Yang<sup>1,4</sup>

7

8 <sup>1</sup>Department of Geology, University at Buffalo, 126 Cooke Hall, Buffalo, NY 14260, USA

9 <sup>2</sup>New York State Geological Survey, New York State Museum, 222 Madison Ave, Albany, NY 12230, USA

10 <sup>3</sup>Department of Geoscience, Utah State University, 4505 Old Main Hill, Logan, UT 84322, USA

11 <sup>4</sup>Oak Ridge Institute of Science and Education, 1299 Bethel Valley Road, Oak Ridge, TN, 37830 USA

12

13 *Correspondence to:* Karlee K. Prince ([karleepr@buffalo.edu](mailto:karleepr@buffalo.edu))

14 **Abstract.** The timing of the last deglaciation of the Laurentide Ice Sheet in western New York is poorly constrained.  
15 The lack of direct chronology in the region has led to a ~~provocative~~ hypothesis that the Laurentide Ice Sheet  
16 re-advanced to near its Last Glacial Maximum terminal position in western New York at ~13 ka, which challenges  
17 long-standing datasets. To address this hypothesis, we obtained new chronology from the Kent (terminal) and Lake  
18 Escarpment (first major recessional) moraines using radiocarbon ages in sediment cores from moraine kettles  
19 supplemented with two optically stimulated luminescence ages ~~from topset beds in an ice-contact delta~~. The two  
20 optically stimulated luminescence ages date the Kent (terminal) position to  $19.8 \pm 2.6$  and  $20.6 \pm 2.9$  ka. ~~Within the~~  
21 ~~sediment cores from both moraines, the lowest reliable radiocarbon ages range from 15,000–15,400 to~~  
22 ~~13,600–14,000 cal yr BP. Below these dated levels is~~ Within the sediment cores, there is sedimentologic evidence of  
23 an unstable landscape during basin formation ; radiocarbon ages from the lowest sediments in our cores are not in  
24 stratigraphic order and date from 19,350-19,600 to 14,050-14,850 cal yr BP. We interpret these ages as loosely  
25 minimum-limiting constraints on ice sheet retreat. Our oldest radiocarbon age of 19,350-19,600 cal yr BP – from a  
26 rip-up clast – suggests ice-free conditions at that time. Above the lowest sediments there is organic-rich silt and  
27 radiocarbon ages in stratigraphic order . We interpret the lowest ages in these organic-rich sediments as  
28 minimum-limiting constraints on kettle basin formation. The lowest radiocarbon ages from organic-rich sediments  
29 from sites on both Kent and Lake Escarpment moraines range from 15,000-15,400 to 13,600-14,000 cal BP. We  
30 interpret ~~that~~ the 5 kyr lag between the optically stimulated luminescence ages and kettle basin formation ~~the lowest~~  
31 ~~reliable radiocarbon ages~~ as the result of persistent buried ice in ice-cored moraines until ~15 to 14 ka. The cold  
32 conditions associated with Heinrich Stadial 1 may have enabled the survival of ice-cored moraines until after 15 ka,  
33 and in turn, climate amelioration during the Bølling Period (14.7 – 14.1 ka) may have initiated landscape  
34 stabilization. This model potentially reconciles the sedimentological and chronological evidence underpinning the  
35 ~~provocative~~ re-advance hypothesis, which instead could be the result of moraine instability and sediment  
36 mobilization during the Bølling-Allerød periods (14.7 – 13 ka). Age control for future work should focus on features  
37 that are not dependent on local climate.

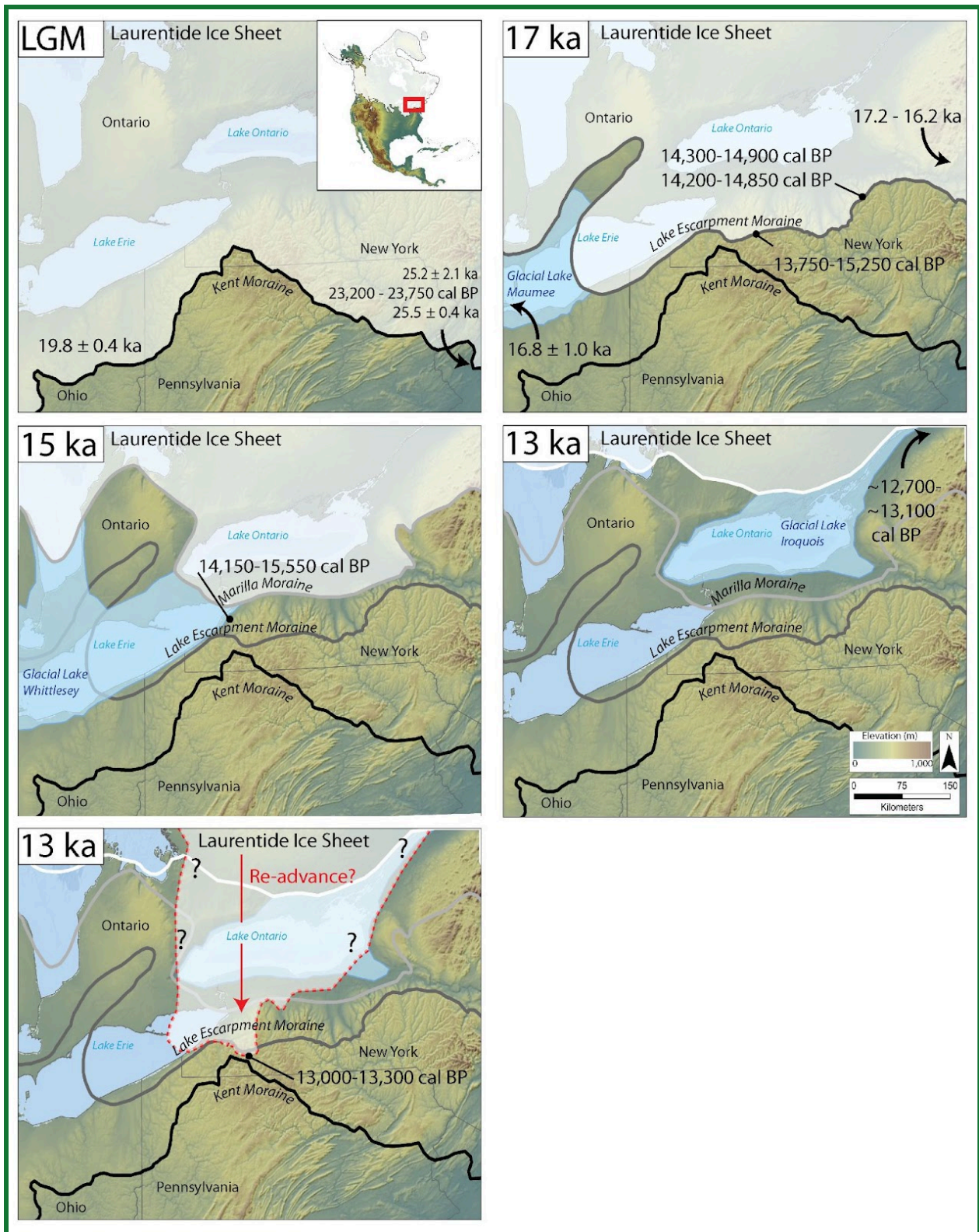
38

## 39 1 Introduction

40 Much glacial research over the last century has focused on the style and timing of Laurentide Ice Sheet  
41 (LIS) recession from the Great Lakes region of North America following the Last Glacial Maximum (LGM, 26-19  
42 ka; Dalton et al., 2020; Dyke, 2004; Fairchild, 1909). Well constrained ice sheet chronologies are necessary to  
43 ~~determine~~ ~~constrain~~ the timing of meltwater re-routing events from ice-dammed lakes that occupied the Great Lakes  
44 basins during the last deglaciation (Barth et al., 2019; Calkin and Feenstra, 1985; Leydet et al., 2018; Porreca et al.,  
45 2018; Rayburn et al., 2007), as these events are hypothesized to have had significant climatic impacts (Broecker et  
46 al., 1989; Donnelly et al., 2005). Models that attempt to understand past climate change (Osman et al., 2021), ice  
47 sheet sensitivity (Briner et al., 2020), and atmospheric organization (Löfverström et al., 2014; Tulenko et al., 2020)  
48 all require paleo ice sheet configurations. Therefore, well-defined ice sheet retreat chronologies are critical for  
49 understanding dynamics and forcings within the late glacial climate system.

50 Despite the critical need for precise chronologies of ice margin retreat of the LIS in the Great Lakes region,  
51 ice margin reconstructions in western New York lack detailed age control. Here, there are no local ages on the  
52 terminal moraine and few from the recessional moraines (Muller and Calkin, 1993), leaving the deglacial  
53 chronology to be largely based on correlations with dated moraines and proglacial shorelines to the west in Ohio and  
54 to the east in New York (Fullerton, 1980; Ridge, 2003). These correlations suggest that the western New York Kent  
55 (terminal) and Lake Escarpment (recessional) moraines date to ~20 and 17 ka, respectively (Fig. 1). However,  
56 Young et al. (2020) recently interpreted new and existing radiocarbon ages from western New York to support a  
57 significant re-advance of the LIS at ~13 ka that overtopped the Lake Escarpment Moraine and nearly reached the  
58 Kent Moraine (Fig. 1). The evidence includes the re-interpretation of several unrelated sites throughout western New  
59 York, but largely hinges on new trenched sediment sections near the Kent Moraine revealing logs in clayey  
60 diamicton, which Young et al. (2020) suggest requires glacial overriding of a forest ~13.3 to 13.0 ka. In contrast to  
61 Young et al.'s (2020) reconstruction, most literature places the LIS margin north of Lake Ontario at this time (Dalton  
62 et al., 2020; Muller and Calkin, 1993; Terasmae, 1980; and references therein), with the drainage of Glacial Lake  
63 Iroquois occurring at ~13 ka (Fig. 1; Cronin et al., 2012; Lewis and Anderson, 2019; Rayburn et al., 2005). To  
64 reconcile the disagreement in timing between the hypothesized re-advance and existing chronologies, Young et al.  
65 (2020) invoke a largely floating ice mass that left minimal traces of its existence in most areas. If a re-advance of the  
66 scale hypothesized by Young et al. (2020) occurred (henceforth referred to as the 'Allerød re-advance hypothesis'),  
67 there would be a need to revisit many regional deglaciation chronologies.

68 To further constrain moraine ages in western New York and to test the Allerød re-advance hypothesis, we  
69 obtained 23 new macrofossil-based radiocarbon ages from five sediment cores collected on the Kent Moraine, and  
70 18 new macrofossil-based radiocarbon ages from two sediment cores on the Lake Escarpment Moraine. The Lake  
71 Escarpment Moraine is within the extent of the proposed re-advance, so if basal ages from sites on this moraine  
72 pre-date ~13 ka, and the subsequent stratigraphy shows no evidence of a re-advance, then the evidence would refute  
73 the Allerød re-advance hypothesis. Conversely, basal radiocarbon ages that post-date ~13 ka, and/or evidence that  
74 the sediment stratigraphy is interrupted at ~13 ka, would support an Allerød re-advance. Additionally, we obtained  
75 two optically stimulated luminescence (OSL) ages from kame delta sediments associated with deposition of the Kent  
76 Moraine to provide a more complete understanding of deglaciation. Our results provide new chronological  
77 constraints in the western New York data gap, and do not support the ~13 ka re-advance proposed by Young et al.  
78 (2020). Rather, our data support a model of initial moraine deposition followed by thousands of years before kettle  
79 basin formation and final moraine stabilization.



80

81 Figure 1. Map depictions of the deglaciation of the eastern Great Lakes after the Last Glacial Maximum. Black line is the  
 82 Kent Moraine, modified from Dalton et al. (2020), the 'Pennsylvania Department of Conservation and Natural Resources  
 83 Late Wisconsin Glacial Border' (<https://www.pasda.psu.edu>), and the 'Quaternary Geology 500K - Glacial Boundary of  
 84 Ohio' (<https://gis.ohiodnr.gov>).

85 Escarpment Moraine. Light gray line is the 15 ka ice margin from Dalton et al. (2020) which depicts the Marilla Moraine.  
86 Glacial Lake Maumee and Whittlesey are included for general reference, and ~~drawn~~<sup>derived</sup> with shoreline elevations  
87 (Fisher et al., 2015). White line is the 13 ka ice margin from Dalton et al. (2020) and we estimated Glacial Lake Iroquois  
88 using Bird and Kozłowski (2016). Red dashed line depicts a hypothesized ice sheet configuration to explain the hypothesis  
89 presented in Young et al. (2020). Note that the LIS would dam a pro-glacial lake in the Lake Erie basin and overrun  
90 several moraine belts, including the Lake Escarpment Moraine. Radiocarbon, cosmogenic nuclide, and OSL ages  
91 discussed in the text are shown with approximate locations. Arrows indicate study sites are off the map extent. Panel  
92 LGM: Glover et al. (2011), Corbett et al. (2017), Stanford et al. (2020), Balco et al. (2009), and Balco et al. (2002). Panel 17  
93 ka: Fisher et al. (2015), Fritz et al. (1987), Kozłowski et al. (2018), and Ridge (2003). Panel 15 ka: Calkin and McAndrews  
94 (1980). Panels 13 ka: Lewis and Anderson (2019), Rayburn et al. (2007), Richard and Occhietti (2005), and Young et al.  
95 (2020). -DEM from U.S. Geological Survey's Center for Earth Resources Observations and Science (EROS).

96

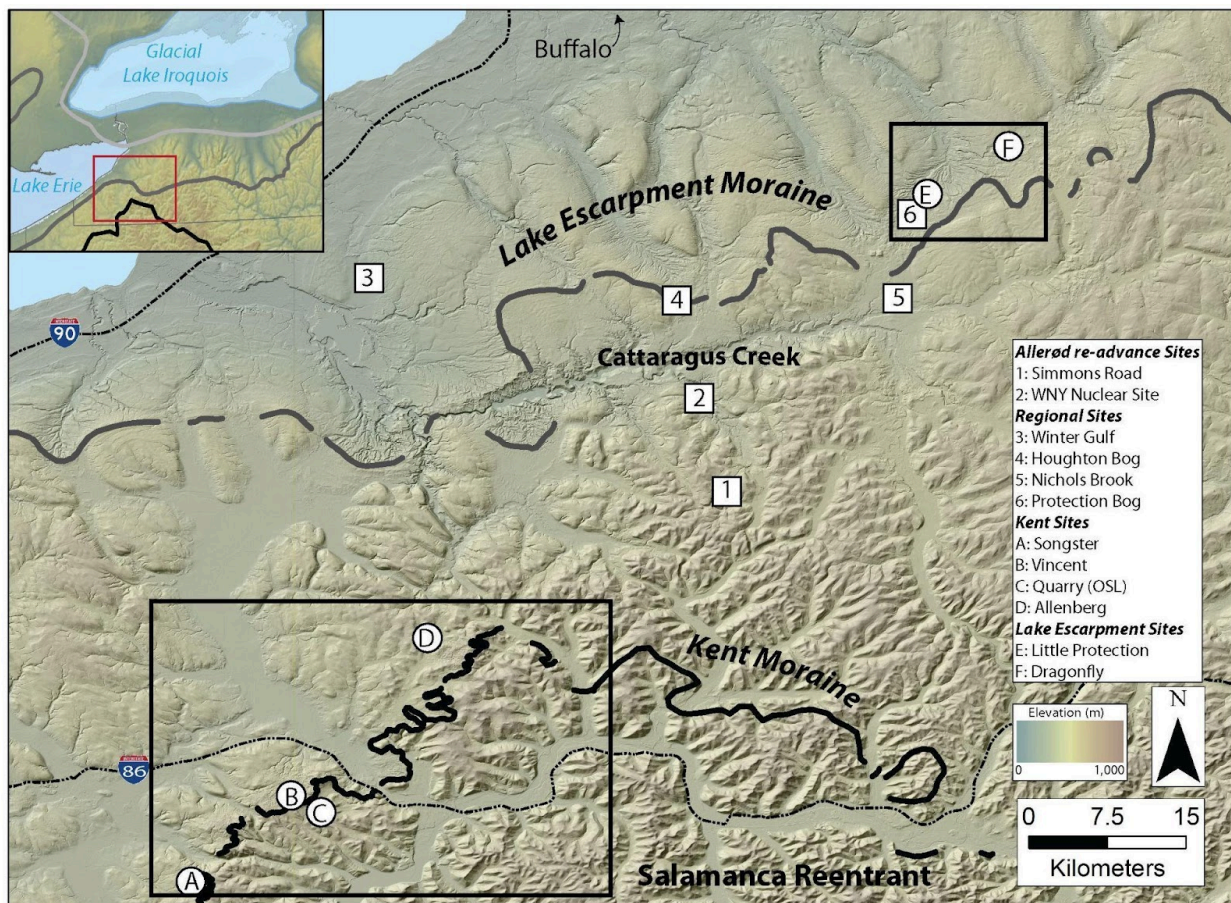
## 97 2 Geologic Setting

98 The Kent Moraine in western New York is correlated to the Kent Moraine in northwest Ohio, the Olean  
99 Moraine in Pennsylvania, the Harbor Hill Moraine in New Jersey, and the Martha's Vineyard Moraine in  
100 Massachusetts (Fig. 1; Balco et al., 2002; Fullerton, 1980; Muller and Calkin, 1993; Stanford et al., 2020). Retreat  
101 from the LGM moraine in these adjacent regions is dated to  $19.8 \pm 0.4$  ka in Ohio (Glover et al., 2011),  $25.2 \pm 2.1$  ka  
102 (Corbett et al., 2017) and 23,200-23,750 cal-yr BP in New Jersey (Stanford et al., 2020), and  $25.5 \pm 0.4$  ka in  
103 Massachusetts (Balco et al., 2009; Balco et al., 2002). Therefore, we infer that the Kent Moraine in western New  
104 York was likely deposited sometime between 25 and 20 ka.

105 The first major moraine belts deposited after the maximum LGM position were the Ashtabula Moraine in  
106 Ohio and northwest Pennsylvania, the Lake Escarpment Moraine in western New York, and Valley Heads moraines  
107 in central New York (Fig. 1; Fullerton, 1980; Muller and Calkin, 1993). During this ice position, Glacial Lake  
108 Maumee occupied the Lake Erie basin ~~around~~<sup>around</sup>, and is dated to 17,000 - 16,000 cal-ka BP based ~~y~~<sup>y</sup> on radiocarbon  
109 dating at the paleo-outlet and OSL dating of strandlines (Calkin and Feenstra, 1985; Eschman and Karrow, 1985;  
110 Fisher et al., 2015). Ridge (2003) tied the outer and inner Valley Heads moraines to the New England Varve  
111 Chronology, placing these moraines at 17,200 and 16,200 cal-yr BP, respectively. Kozłowski et al. (2018) report  
112 basal ages of 14,300-14,900 and 14,200-14,850 cal yr BP from basins within the outer Valley Heads limit. These  
113 ages are younger than previous estimates, leading Kozłowski et al. (2018) to suggest the moraine may have been  
114 re-occupied. ~~Fritz et al. (1987) Calkin and McAndrews (1980)~~ report minimum-limiting radiocarbon ages of  
115 13,750-15,250 cal yr BP from wood ~~within lake deposits~~<sup>within lake deposits</sup> stratigraphically above outwash sands from Nichols Brook  
116 in western New York (Fig. 2). Muller and Calkin (1993) extrapolated their ages to estimate  $\sim 17,600$  cal yr BP for the  
117 emplacement of the outwash.

118 Following the deposition of the Lake Escarpment Moraine, Glacial Lakes Whittlesey and Warren occupied  
119 the Lake Erie basin between 16 and 14 ka (Fig. 1; Fullerton, 1980; Muller and Calkin, 1993). The lowering of  
120 Glacial Lake Whittlesey to Glacial Lake Warren is dated to 14,150-15,550 cal yr BP at Winter Gulf in western New  
121 York (Fig. 2; Calkin and McAndrews, 1980), and Warren strandlines in northwest Ohio have been dated to  $14.2 \pm$   
122  $1.3$  ka (Higley et al., 2014) and  $14.1 \pm 1.0$  ka in (Campbell et al., 2011). These proglacial lake chronologies provide  
123 unambiguous minimum age constraints of  $>15$  ka for the deposition of the Lake Escarpment Moraine.

124 The LIS continued its northward retreat and formed Glacial Lake Iroquois from 14.7 to 13.0 ka in the Lake  
 125 Ontario basin (Fig. 1; Muller and Calkin, 1993; Muller and Prest, 1985; Teller, 2003). The switch of the Glacial  
 126 Lake Iroquois spillway from the Mohawk River valley to the lower outlet at Covey Hill is constrained between  
 127 13,200 and 13,000 cal yr BP by numerous radiocarbon constraints from the pre- and post-flood histories of Lake  
 128 Vermont and Lake Iroquois (Lewis and Anderson, 2019; Rayburn et al., 2007; Richard and Occhietti, 2005).  
 129 Similarly, the formation of the Champlain Sea occurred between 13,100 and 12,700 cal yr BP, which post-dates the  
 130 final draining of Glacial Lake Iroquois and requires an ice margin north of the Lake Ontario outlet (Cronin et al.,  
 131 2012; Rayburn et al., 2011). Collectively, this ice recession chronology is at odds with the Allerød re-advance  
 132 hypothesis, with its significant LIS advance across the Lake Ontario basin and to near the terminal moraine in  
 133 western New York ~13 ka (Fig. 1; Young et al., 2020).



134  
 135 Figure 2. Study sites in relation to previously published work. Black and gray lines are the same as in Fig. 1. Squares 1  
 136 and 2 depict hypothesized sites overrun by the Allerød re-advance at 13 ka (Young et al., 2020). Circles A-D are our sites  
 137 on the Kent Moraine. Circles E and F are our sites on the Lake Escarpment Moraine. Squares 3-6 are Winter Gulf and  
 138 Nichols Brook (Calkin and McAndrews, 1980), and Houghton and Protection Bog (Miller, 1973). The two black boxes  
 139 show the extent of the maps in Fig. 3. DEM from U.S. Geological Survey's Center for Earth Resources Observations and  
 140 Science (EROS).

141

## 142 3 Methods

### 143 3.1 Sediment cores

144 Our primary approach for constraining the timing of deglaciation and testing the Allerød re-advance  
145 hypothesis was obtaining basal sediment ages from kettles within the Kent and Lake Escarpment Moraines. Newly  
146 available light detection and ranging (LiDAR)-based bare-Earth 1-m digital elevation models (DEMs) enabled us to  
147 identify natural kettle basins (Fig. 3). Typically, moraines in western New York have both single ridges where the ice  
148 sheet abutted higher topography, and hummocky moraine belts that contain numerous kettle basins. Kame deltas  
149 exist in places where the ice sheet dammed adjacent river valleys. The hummocky nature of most moraines indicates  
150 that the moraines were ice-rich when deposited (Fig. 3).

151 We collected sediment cores from kettles that presently range from bogs to wetlands. We cored five sites on  
152 the Kent Moraine referred to as the Vincent-1 (core name: 20VIN1), Vincent-3 (20VIN3), Vincent-4 (20VIN4),  
153 Songster (21SONG1), and Allenberg (15ABB7) sites (Table 1, Fig. 3), and two sites on the Lake Escarpment  
154 Moraine referred to as the Little Protection (21LPB1) and Dragonfly (13DFK1) sites (Table 1, Fig. 3). All sites are  
155 within hummocky moraine.

156 We determined basin depocenters using thin steel rods to measure the depth of the organic sediment infill.  
157 In the depocenter, we used Livingstone- and Russian Peat-style corers to collect organic-rich sediment infill, and a  
158 manual percussion GeoProbe system to collect the underlying stiff, minerogenic sediments. From some sites, our  
159 sediment cores extended from the present surface to mineral-rich sediments below the organic-sediment infill; from  
160 others, our sediment cores began and ended at depth, spanning the organic-to-mineral sediment contact and  
161 downward until we penetrated coarse deposits (Table 1). We returned and cored the Vincent-1 and -4 sites multiple  
162 times to collect the entire sequence.

163 We split, imaged, and generated downcore data on all sediment cores at the University at Buffalo. We  
164 measured magnetic susceptibility in contiguous 1 cm intervals using a Bartington MS2E High Resolution Surface  
165 Scanning Sensor scanner connected to a Bartington MS2 Magnetic Susceptibility Meter to assess the minerogenic  
166 content. We calculated loss-on-ignition (LOI) percent by burning  $\sim 1$  cm<sup>3</sup> of sediment in a Thermolyne Muffle  
167 Furnace at successively higher temperatures for water (105°C), organic carbon (550°C), and carbonate (950°C)  
168 content to help characterize the sediment units and depositional setting (Heiri et al., 2001; Last and Smol, 2001). To  
169 calculate composite core length, we spliced together overlapping sediment sections using visual lithologic changes  
170 and magnetic susceptibility measurements. We volumetrically sampled portions of the Little Protection sediment  
171 cores to determine sediment bulk density; these data are used to check for overcompaction during an Allerød  
172 re-advance. The data are only from Little Protection because Dragonfly data creation took place previous to Young  
173 et al. (2020) and we did not measure bulk density.

174 We use radiocarbon dating of macrofossils for age control (Table 2). The sediments are organic-rich in the  
175 upper portions of the cores and are organic-poor in the lower sections. Where available, we picked full plant  
176 macrofossils. We picked macrofossils that were from the center of the sediment core and demonstrably in-situ. In  
177 macrofossil-devoid sections, we wet sieved sediment with deionized water to isolate and combine the largest

178 macrofossil fragments for dating. We attempted to identify macrofossils, but some macrofossil fragments were small  
 179 and unidentifiable (Table 2). We rinsed samples with deionized water, freeze-dried them, and sent samples to the  
 180 National Ocean Sciences Accelerator Mass Spectrometry (NOSAMS) or the Keck Lab at the University of  
 181 California Irvine (KCCAMS) for radiocarbon analysis. ~~We submitted untreated macrofossils, therefore~~ The  
 182 facilities conducted acid-base-acid (ABA) pretreatments, converted samples to graphite, and ran them on the AMS  
 183 (Elder et al., 2019; Olsson, 1986; Pearson et al., 1997; Shah Walter et al., 2015; Vogel et al., 1984).

184 In Table 2, ~~we~~ We report the ~~entire~~ 2 $\sigma$  age range and round ages according to Stuiver and Polach (1977)  
 185 (Table 2). We calibrated all the radiocarbon results using Calib8.1 with the IntCal20 dataset (Reimer et al., 2020;  
 186 Stuiver and Reimer, 1993). All radiocarbon ages in the text were recalibrated with IntCal20.  $\delta^{13}\text{C}$  measurements  
 187 were measured on a split of the  $\text{CO}_2$  gas generated from each sample on an isotope-ratio mass spectrometer.  
 188 Uncertainties in the  $\delta^{13}\text{C}$  from both labs are  $<0.1\%$ . We report  $\delta^{13}\text{C}$  values as ‰ VPDB.

189

Table 1: Site location, core lengths, and ownership.

Site Name	Core Name	Latitude (DD)	Longitude (DD)	Elevation (m asl)	Site Length (m)	Core Top (m bg)	Core Bottom (m bg)	Property Ownership
Vincent 1	20VIN1	42.109	-79.000	596	145.0	0.0	6.6	Vincent Family
Vincent 3	20VIN3	42.110	-78.999	593	39.0	1.5	2.9	Vincent Family
Vincent 4	20VIN4	42.109	-78.999	594	81.0	3.1	5.4	Vincent Family
Songster	21SONG1	42.040	-79.079	581	172.0	4.1	4.8	Songster Family
Allenberg	15ABB7	42.252	-78.883	524	321.0	8.0	14.6	Buffalo Audubon Society
Little Protection	21LPB1	42.621	-78.463	440	228.0	0.0	8.1	Erie County Parks Dept.
Dragonfly	13DFK1	42.679	-78.386	450	117.0	0.0	7.3	Buffalo Audubon Society
Corbett Hill	-	42.114	-78.946	530	-	-	-	JMI Corbett Hill Gravel

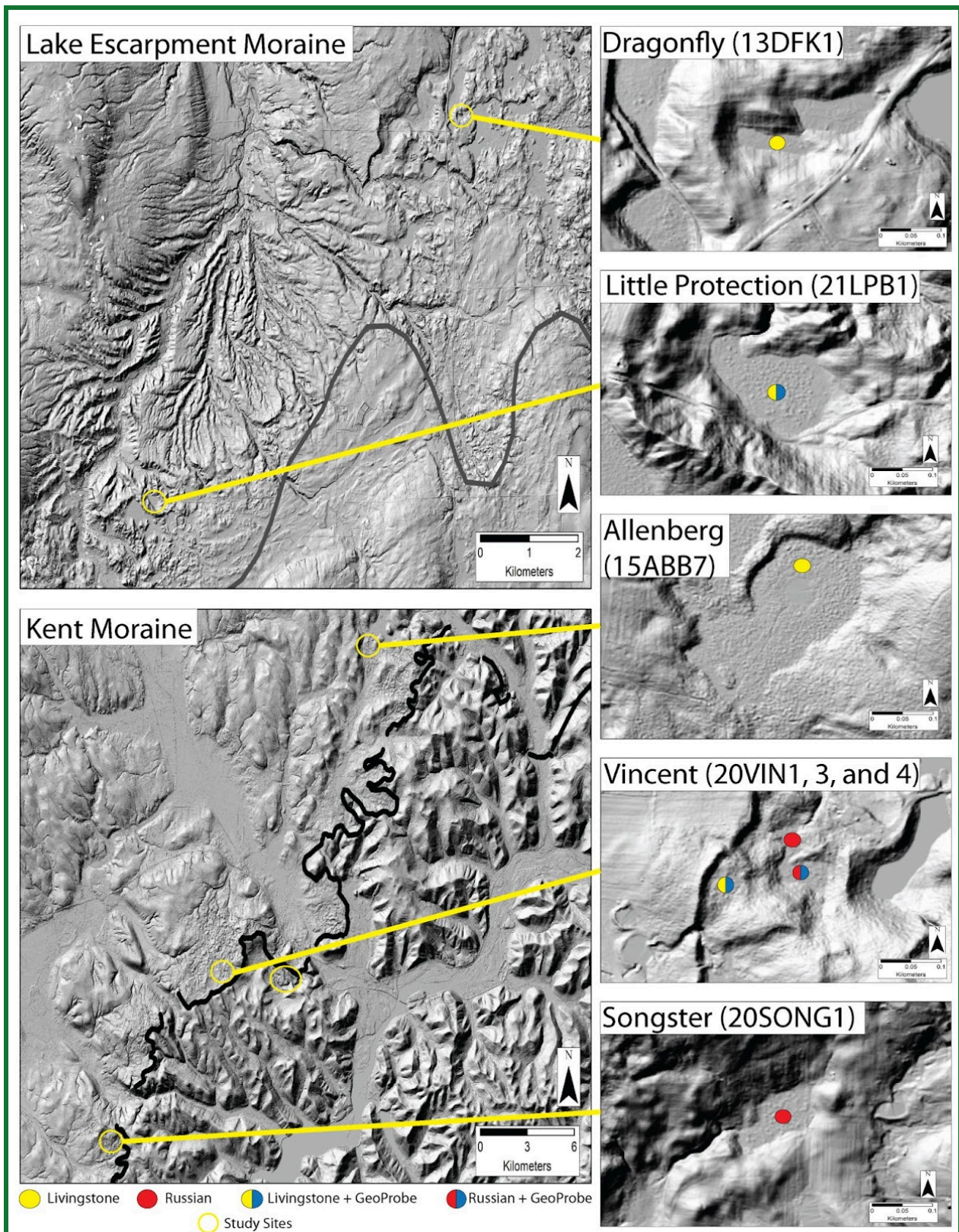
DD: Decimal Degrees

asl: Above sea level

bg: Below ground

190





194 associate each site location with a site map. Figure 4 contains the site map for the open yellow circle with no associated site  
195 map. The filled circles indicate the type of coring device used in each site and the coring location. The filled yellow circles  
196 depict where we used a Livingstone. The filled red circles depict where we used a Russian Peat Corer. The filled  
197 semi-circles indicate where we used a Livingstone or Russian Peat Corer in the soft sediment infill and then used the  
198 GeoProbe in the stiff minerogenic sediment.

199

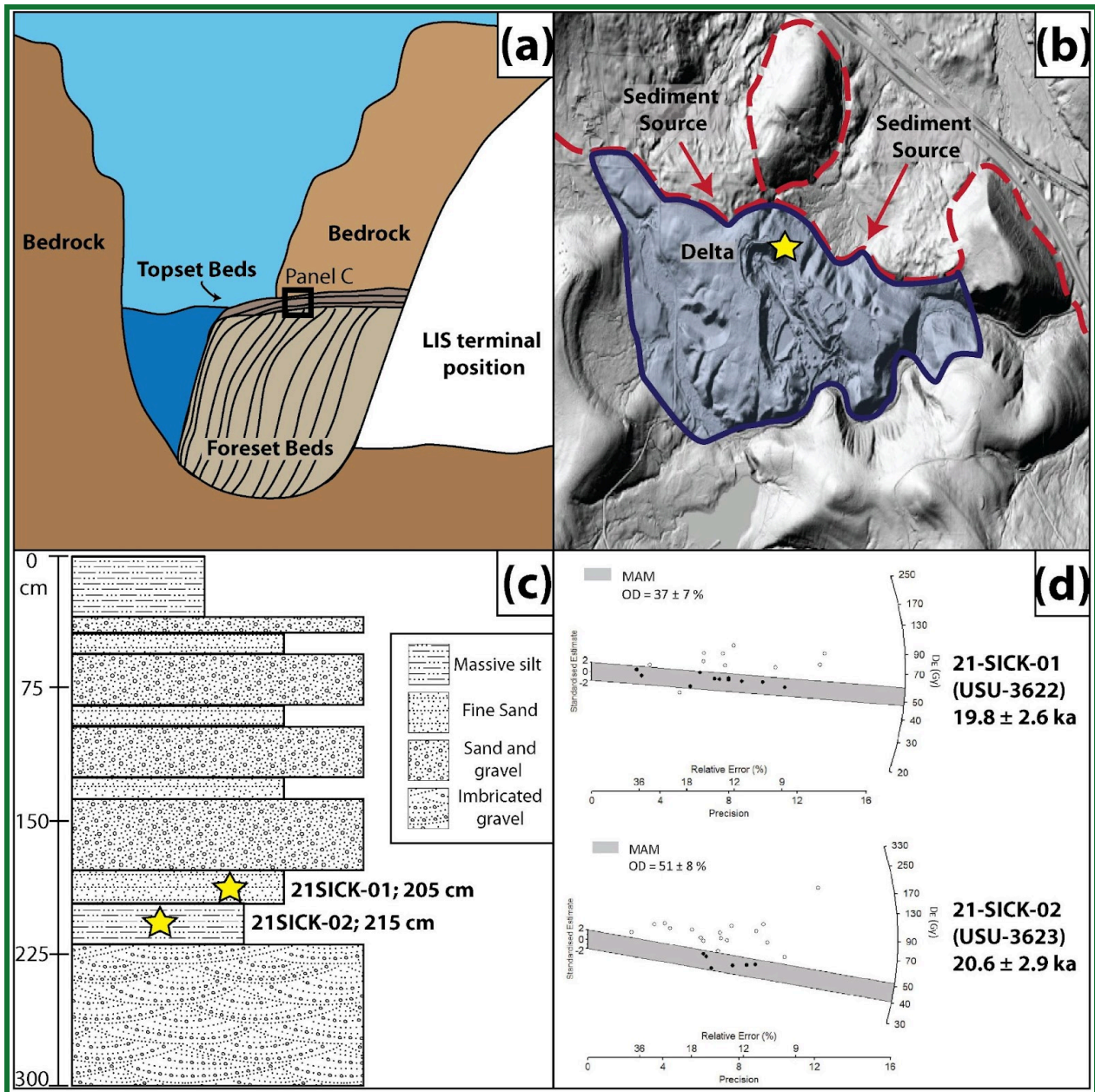
### 200 3.2 Optically stimulated luminescence dating

201 We collected sediment samples for OSL dating from topset beds within an ice-contact delta deposit  
202 associated with the Kent Moraine to determine when the LIS was present at this location (Fig. 3 & 4). Our sample  
203 location was Corbett Hill Gravel Quarry, an active aggregate quarry that exposes large sedimentary sequences  
204 indicative of a proglacial delta. The sediments consisted of cobble-rich foreset beds overlain by ~3 m of  
205 near-horizontal topset beds. We collected sand samples for OSL dating from the topset sequence ~2.1 m below the  
206 delta surface. We created a fresh exposure of the topset beds with an excavator, exposing alternating layers of  
207 gravels and coarse sands, with lenses of medium/fine-sand and silt. We collected two samples for OSL dating in  
208 fine-sand lenses in 5.1 x 25.4 cm (2 x 10 inch) aluminum tubes after clearing back outer sediments (Fig. 4). Samples  
209 for water content and dose rate determination were collected from surrounding sediments.

210 We processed the samples at the Utah State University Luminescence Laboratory for small aliquot OSL  
211 dating of fine-grained quartz sand (Table 3, Table SA1). First, we purified samples to 150-250  $\mu\text{m}$  quartz sand using  
212 wet sieving, and chemical treatment with 10% hydrochloric acid to remove carbonates, 5% peroxide to remove  
213 organics, 2.72  $\text{g}/\text{cm}^3$  sodium polytungstate to remove heavy minerals and 48% hydrofluoric acid to remove feldspars  
214 and etch the quartz grains. We analyzed small aliquots of quartz (0.4 to 1 mm diameter of sand mounted on disk,  
215 ~10-20 grains) on Risø DA-20 readers, using the single-aliquot regenerative-dose (SAR) protocol (Murray and  
216 Wintle, 2000). We analyzed 42 aliquots for sample 21SICK-01 and 37 for sample 21SICK-02, of which we used 21  
217 and 23 aliquots for age calculations, respectively (Fig. 4A1 & A2S7). Aliquots were rejected from age calculation if  
218 they showed signal depletion with infrared stimulation indicating feldspar contamination (0-12 aliquots), poor  
219 recycling of a repeat point (greater than 80% difference between repeat points, 7-8 aliquots), high recuperation of a  
220 zero-dose point (>10% of the Natural signal, 0-6 aliquots), extrapolation of the equivalent dose beyond the  
221 dose-response curve (0-2 aliquots) and poor dose-response curve fit (0-3 of aliquots). We applied a minimum age  
222 model (MAM) to the samples to calculate our equivalent doses ( $D_E$ ; Grays; Gy, Fig. 4A1 & S7A2), as used by similar  
223 studies on LIS glaciofluvial terraces elsewhere in the northern United States (Rittenour et al., 2015). MAM's are  
224 useful in these glaciofluvial environments because of the increased potential for incomplete bleaching from  
225 subglacial or turbid water sediment transport.

226 We determined the dose rate for OSL age calculation based on U, Th, K, and Rb concentrations from the  
227 surrounding sediments using inductively coupled plasma-mass spectrometry and atomic emission spectrometry.  
228 Using the conversion factors of Guérin et al. (2011), we converted elemental concentrations to dose rate. The  
229 contribution of cosmic radiation was based on sample depth, elevation and latitude following Prescott and Hutton  
230 (1994). We also determined water content by measuring the mass of the samples before and after desiccation. With  
231 these three factors, we were able to calculate environmental dose rates (Gy/kyr). Our reported OSL ages are simply

232 the  $D_E$  (determined with the MAM) divided by the dose rate with  $1\sigma$  standard error (Table 3). We report ages with  
 233  $1\sigma$  uncertainty (Table 3).



234

235 Figure 4. Panel A) is a schematic of the kame delta creation. The LIS dammed a lake and deposited the delta outboard of  
 236 the Kent Moraine. B) is a 1-m DEM hillshade showing the kame delta outboard of the Kent Moraine (within the open  
 237 yellow circle in Fig. 3). Red dashed line depicts the extent of the Kent Moraine. Red arrows depict the sediment source for  
 238 the delta. Blue line and shading depicts the delta deposit. Yellow star on the side of the active quarry shows our sampling  
 239 site. C) shows a stratigraphic column of the topset beds. We use the FGDC Digital Cartographic Standard for Geologic  
 240 Map Symbolization (U.S. Geological Survey). Yellow stars show our sampling location. D) is a field photo of the  
 241 stratigraphic section showing the location of our two samples. Equivalent dose ( $D_E$ ) distributions for the luminescence  
 242 samples collected from the kame delta associated with an ice-margin position near the Kent moraine. MAM = minimum  
 243 age model of Galbraith and Roberts (2012) fit to the  $D_E$  data (gray shaded region). OD = overdispersion, a metric of  $D_E$   
 244 scatter beyond instrumental error, where  $OD > 30\%$  is interpreted to be due to partial bleaching due to incomplete solar  
 245 resetting of the luminescence signals in the quartz grains.

246

## 247 **4 Results**

### 248 **4.1 Stratigraphy and Radiocarbon Results**

#### 249 **Vincent-1 (Kent Moraine)**

250           The bottom 2.5 m is a gray massive pebbly diamicton with a silty matrix that we call Unit 1. We only  
251 recovered Unit 1 at this study site and collected it with the Geoprobe system (Fig. 5). There is a sharp contact with  
252 layered gray sand and silt that grades to alternating massive brown and gray silt with sparse macrofossils. We call  
253 this Unit 2. There is a sharp contact with massive dark brown organic-rich silt that we call Lower Unit 3. In the  
254 initial sediments of Lower Unit 3, there are three layers of gray silt and an inclusion of gray clay that are identical to  
255 the sediment of Unit 2. There is a sharp contact with peat which continues to the top of the core that we call Upper  
256 Unit 3. Broadly, this sediment progression is found in the other six sediment cores from both moraines so we use the  
257 Unit 2 and 3 terminology for them as well. Figures 5a and 5b depict the downcore data. For the other six sediment  
258 cores, magnetic susceptibility values are higher in Unit 2 than Unit 3, water and organic carbon content values are  
259 lowest in Unit 2, rise in Lower Unit 3, and are highest in Upper Unit 3, and calcium carbonate remains below 8% in  
260 all sediment cores so it is not plotted in Fig. 5.

261           Figure 5 and Supplementary Figure 1 show the ten radiocarbon ages from 20VIN1. The seven ages in Unit  
262 2 are from combined macrofossils and have little stratigraphic order. The three ages in Unit 3, from single  
263 macrofossils, are in stratigraphic order. 20VIN1 has an age of 15,050-15,550 cal BP from the bottom of Unit 2, yet  
264 is stratigraphically below older ages from Unit 2 of 15,650-15,900, 15,800-16,150, and 16,050-16,300 cal BP. There  
265 is an inclusion of macrofossils at the Unit 2/3 contact that was dated twice and yields two radiocarbon ages from  
266 combined macrofossils of 19,350-19,600 and 14,050-14,850 cal BP; combined macrofossils from the surrounding  
267 sediment produce an age of 14,300-15,050 cal BP. *Picea* seeds from the top of Lower Unit 3 are 13,650-14,050 cal  
268 BP. There are two ages in the Upper Unit 3; a twig that dates to 13,150-13,300 and wood that dates to 8,390-8,520  
269 cal BP.

#### 270 **Vincent-3 (Kent Moraine)**

271           In 20VIN3, Unit 2 begins as gray silt, transitions to a light brown silt, and is topped by gray clay. The  
272 contact with Unit 3 is sharp. Unit 3 is massive organic-rich silt. There is a layer of gray silt in the base of Unit 3.  
273 There are two radiocarbon ages from 20VIN3 (Fig. 5; Fig. S2). The one age in Unit 2 is from combined macrofossils  
274 that date to 14,350 – 15,150 cal BP. The one age at the base of Unit 3 is from combined macrofossils and dates to  
275 15,350 – 15,650 cal BP.

#### 276 **Vincent-4 (Kent Moraine)**

277 In 20VIN4, Unit 2 contains alternating layers of pebbly diamicton (with some clasts up to 5 cm long) and  
278 silty clay. The contacts between the layers are sharp and one is undulating. Unit 3 is a massive organic-rich silt.  
279 There are four radiocarbon ages from Unit 2 (Fig. 5; Fig. S3). The lowest age is from a piece of wood that dates to  
280 14,250 – 15,000 cal BP. Then the next three ages are from combined macrofossils and date to 14,150 – 14,850,  
281 14,300 – 14,900, and 14,300 – 14,900 cal BP.

#### 282 **Songster (Kent Moraine)**

283 In 21SONG1, Unit 2 is silty clay with pebbles. The contact with Unit 3 is sharp. Unit 3 begins with  
284 organic-rich silt with some sand and pebbles. Large macrofossils are common. This grades into organic-rich silt.  
285 One radiocarbon age from a piece of wood in the bottom of Unit 3 dates to 14,350 – 15,050 cal BP (Fig. 5).

#### 286 **Allenberg (Kent Moraine)**

287 In 15ABB7, we did not collect Unit 2. Lower Unit 3 is an organic-rich silt and Upper Unit 3 is peat. There  
288 are four ages from Unit 3 (Fig. 5; Fig. S4). These samples were not identified at the time of dating. The lowest age is  
289 13,800 – 14,050 cal BP. The next 3 ages are in stratigraphic order and range from 12,700 – 12,850 to 795 – 920 cal  
290 BP.

#### 291 **Little Protection (Lake Escarpment Moraine)**

292 In 21LPB1, Unit 2 begins with 2 cm of gray silty gravel before a sharp contact with massive, oxidized sand  
293 and gravel. Above this is a sharp transition to alternating layers of gray silt, silty gravel, and sand; these layers have  
294 sharp and sometimes undulating contacts. That is overlain by massive gray clay. The contact with Unit 3 is gradual  
295 over 3 cm. Lower Unit 3 is an organic-rich silt and Upper Unit 3 is peat. There is one radiocarbon age from Unit 2  
296 on a fish bone that dates to 16,650 – 17,350 cal BP. There are eight radiocarbon ages from Unit 3 (Fig. 5; Fig. S6).  
297 The lowest age is from a piece of wood that dates to 13,600 – 14,000 cal BP. The next seven are in stratigraphic  
298 order and range from 13,350 – 13,600 to 5,580 – 5,650 cal BP. To address the Allerød re-advance hypothesis and  
299 seek evidence of whether the coring sites were overridden, we measured dry bulk density at 1-cm-resolution through  
300 the time interval of hypothesized re-advance. The bulk density decreases from 1.55 g/cm<sup>3</sup> to 0.42 g/cm<sup>3</sup> in the  
301 transition from Unit 2 to 3. (Fig. 5) The density decreases due to the transition from minerogenic silt to organic-rich  
302 silt and remains below 0.42 g/cm<sup>3</sup> into Unit 3.

#### 303 **Dragonfly (Lake Escarpment Moraine)**

304 In 13DFK1, Unit 2 is gray silt. The contact with Unit 3 is sharp. Lower Unit 3 is an organic-rich silt and  
305 Upper Unit 3 is peat. There are nine radiocarbon ages from Unit 3 (Fig. 5; Fig. S5). The lowest age is from grass and  
306 dates to 15,000 – 15,400 cal BP. The next eight radiocarbon ages are in stratigraphic order and range from 13,800 –  
307 14,000 to 4,420 – 4,800 cal BP.

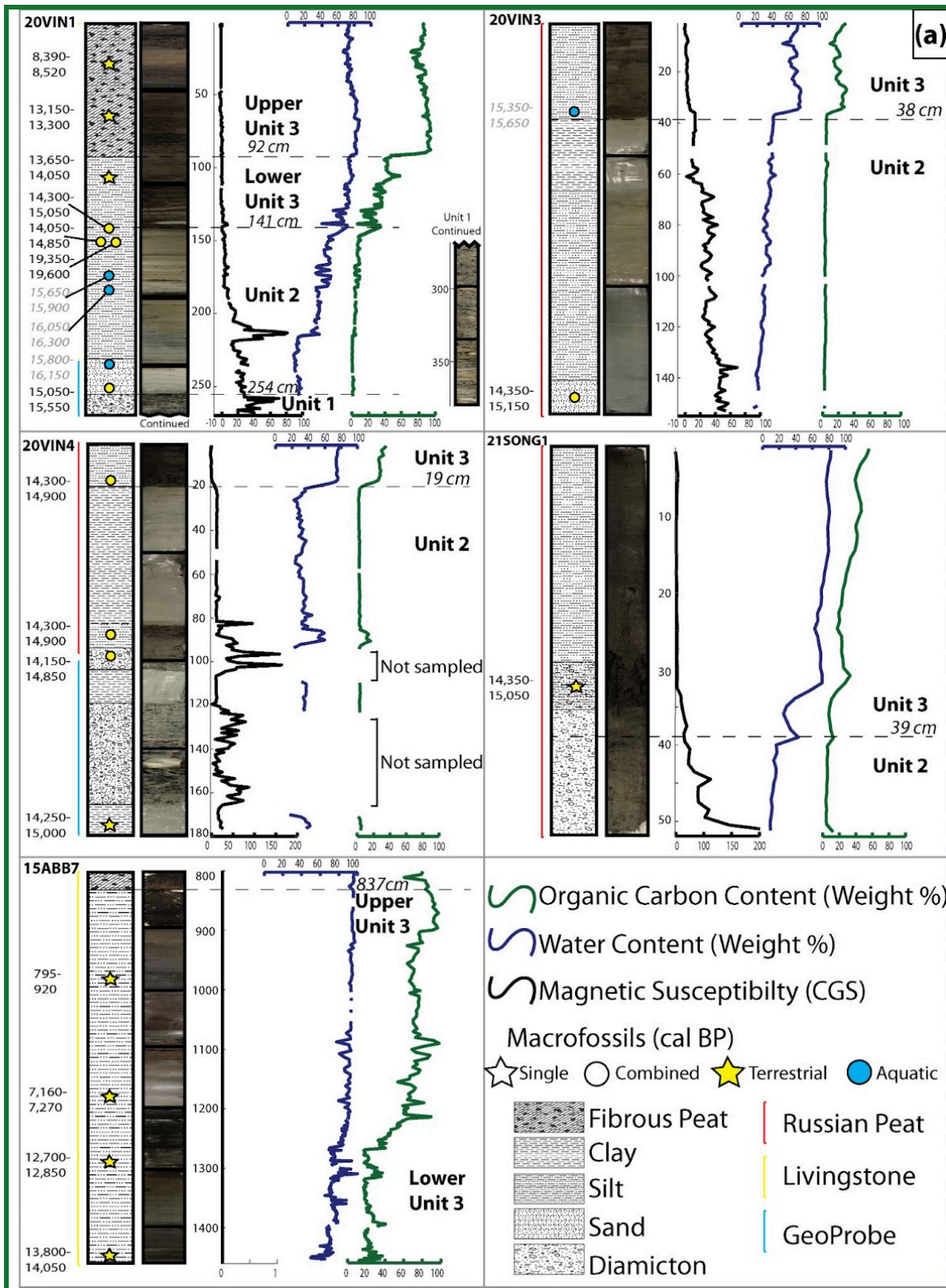
308        ~~The sediment cores contain three stratigraphic units: a basal unit (Unit 1) of diamicton, an intermediate unit~~  
309 ~~(Unit 2) dominated by silt and sand, and an upper unit (Unit 3) of organic rich silt and peat (Fig. 5). We only~~  
310 ~~recovered Unit 1 in 20VIN1 using the Geoprobe system (Fig. 5). Unit 1 is a gray massive pebbly diamicton with a~~  
311 ~~silty matrix. The contact with Unit 2 is sharp.~~¶¶

312        ~~We collected varying thicknesses of Unit 2 (Fig. 5). Unit 2 is mineral rich layers with complex stratigraphy~~  
313 ~~and sparse macrofossil fragments. In 20VIN1, Unit 2 is layered gray sand and silt that grades to alternating massive~~  
314 ~~brown and gray silt (Fig. 5). In 20VIN3, Unit 2 begins as gray silt, transitions to a light brown silt, and is topped by~~  
315 ~~gray clay. In 20VIN4, Unit 2 contains alternating layers of pebbly diamicton (with some clasts up to 5 cm long) and~~  
316 ~~silty clay. The contacts between the layers are sharp and one is undulating. In 21LPB1, Unit 2 begins with 2 cm of~~  
317 ~~gray silty gravel before a sharp contact with massive, oxidized sand and gravel. Above this is a sharp transition to~~  
318 ~~alternating layers of gray silt, silty gravel, and sand; these layers have sharp and sometimes undulating contacts.~~  
319 ~~That is overlain by massive gray clay. In 13DFK1, Unit 2 is gray silt. The contact between Unit 2 and 3 is sharp in~~  
320 ~~all cores.~~¶¶

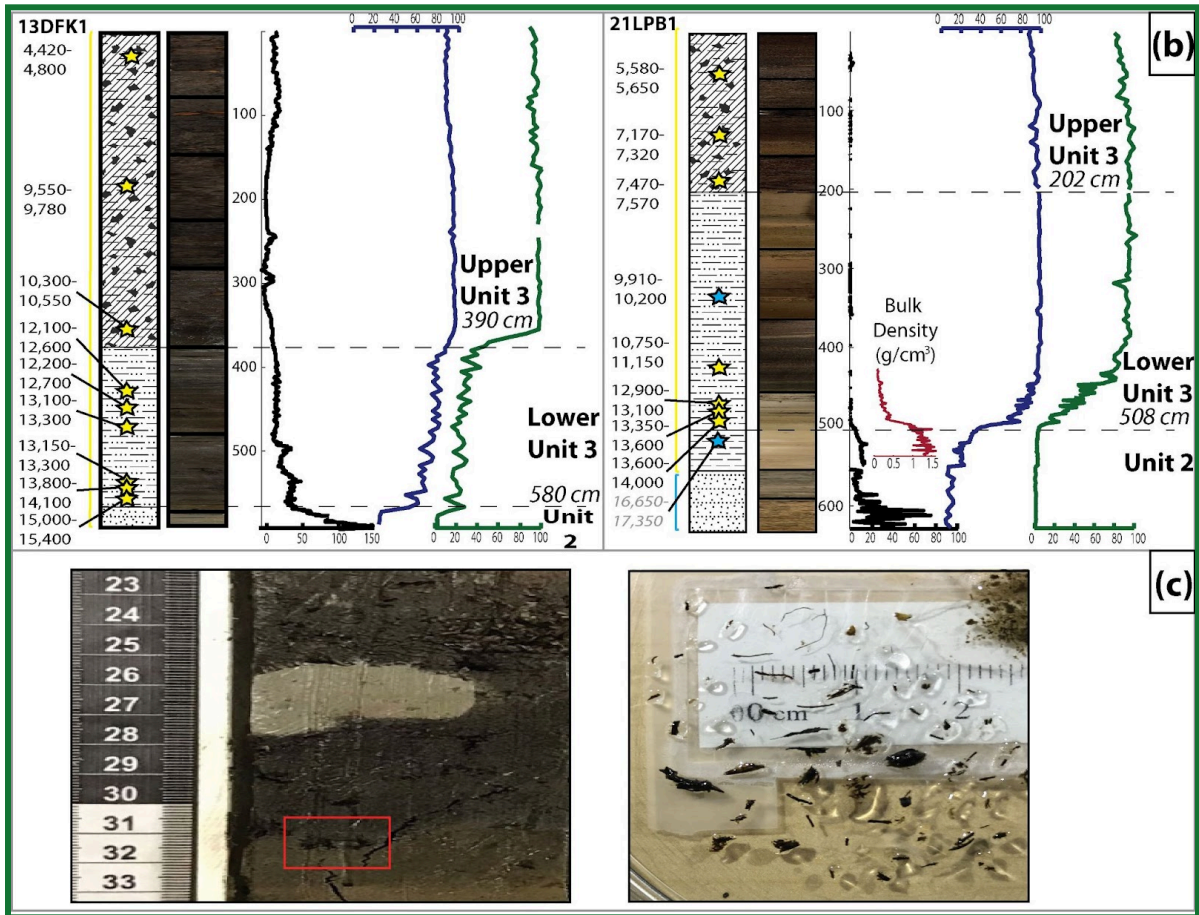
321        ~~Unit 3 is organic rich silt (lower Unit 3) and peat (upper Unit 3) that spans from the mineral layers of Unit~~  
322 ~~2 to the top of each sediment sequence. The transition from organic rich silt to peat is sharp in all cores. In 20VIN1,~~  
323 ~~within the initial sediments of Unit 3, there are three layers of gray silt and an inclusion of gray clay that are~~  
324 ~~identical to the sediment of Unit 2. Similarly, 20VIN3 has a layer of gray silt within the initial organic rich silt. The~~  
325 ~~organic rich silt and peat have high organic carbon content and large macrofossils are common.~~¶¶

326        ~~To address the Allerød re-advance hypothesis and seek evidence of whether the kettle sediments were~~  
327 ~~overridden, we measured dry bulk density at 1 cm resolution through the time interval of hypothesized re-advance~~  
328 ~~in our Little Protection site core (21LPB1). The bulk density decreases from 1.55 g/cm<sup>3</sup> to 0.42 g/cm<sup>3</sup> in the~~  
329 ~~transition from Unit 2 to 3. (Fig. 5) The density decreases due to the transition from minerogenic silt to organic rich~~  
330 ~~silt and remains below 0.42 g/cm<sup>3</sup> into Unit 3.~~

331



332



334

335 Figure 5. Panel A) has the sediment core stratigraphy from the Kent Moraine sites, and B) has the sediment  
 336 core stratigraphy from the Lake Escarpment Moraine sites. We show sediment texture next to the core  
 337 images using the FGDC Digital Cartographic Standard for Geologic Map Symbolization (U.S. Geological  
 338 Survey). We plot magnetic susceptibility (CGS; black line), water content (weight %; blue line), and organic  
 339 content (weight %, green line) by composite depth (cm). The colored line next to the stratigraphic column  
 340 depicts if we used the Russian Peat Corer (red), Livingstone Corer (yellow), or GeoProbe (blue). Stars  
 341 indicate single macrofossils and circles indicate when we combined macrofossils. The yellow filling indicates  
 342 the sample is terrestrial and blue indicates the sample has aquatic macrofossils within it. Yellow stars indicate  
 343 radiocarbon ages presented as the full ( $2\sigma$  range in uncertainty cal yr BP). We used gray text and italics for  
 344 radiocarbon ages we suspect have hardwater contamination. C) is a close-up image of the inferred gray clay  
 345 and macrofossil-rich rip-up clasts in the transition from Unit 2 to 3 in 20VIN1 (shown in red box). The black  
 346 box has post-sieve macrofossils from the rip-up clast in the red box.

347

#### 348 4.2 Sediment core chronology

349 The stratigraphically lowest ages, or basal ages, from the Kent Moraine range from 15,050–15,550 to  
 350 13,800–14,050 cal yr BP (Table 2; Fig. 5). For 20VIN3, 20VIN4, and 21SONG1, the basal ages cluster around  
 351 14,700 cal yr BP. The basal ages from the Lake Escarpment Moraine are 15,000–15,400 and 16,650–17,350 cal yr  
 352 BP. The basal ages are not the oldest ages, however. 20VIN1 has a basal age of 15,050–15,550 cal yr BP, yet is



353 ~~stratigraphically below other ages from Unit 2 of 15,650–15,900, 15,800–16,150, and 16,050–16,300 cal yr BP.~~  
354 ~~Furthermore, 110 cm higher than the basal age, there is an inclusion of macrofossils within Unit 2 that was dated~~  
355 ~~twice and yields two radiocarbon ages of 19,350–19,600 and 14,050–14,850 cal yr BP, combined macrofossils from~~  
356 ~~the surrounding sediment produce an age of 14,300–15,050 cal yr BP. In 20VIN3, the basal age is 14,350–15,150 cal~~  
357 ~~yr BP, yet combined macrofossils higher in the core, at the Unit 2/3 boundary, produce an age of 15,350–15,650 cal~~  
358 ~~yr BP.~~

359

360

Table 2: Radiocarbon dates for each study site. Listed by depth.

Lab Code	Depth (cm)	Material Dated	Mass (mg)	$\delta^{13}\text{C}_{\text{‰}}$	Fraction Modern	Fraction Modern Error	$^{14}\text{C}$ (BP)	$^{14}\text{C}$ error (BP)	2 $\sigma$ age range (cal BP)	
<b>Vincent-1 (20VIN1)</b>										
OS-164770	27.3	Wood	5.8	-26.5	0.3854	0.0015	7,660	30	8,390 8,520	98%
OS-164771	67.3	Twig	5.8	-28.7	0.2441	0.0015	11,350	50	13,150 13,300	97%
OS-164772	109.5-111.0	<i>Picea</i> seeds	75.7	-23.0	0.2263	0.0016	11,950	55	13,650 13,700	6%
OS-164773	145.0	Unidentifiable	2.3	-24.3	0.2105	0.0016	12,500	60	13,750 14,050	91%
UCIAMS-239749	145.2	Moss, unidentifiable	2.4	-28.3	0.1342	0.0007	16,135	45	14,300 14,750	56%
OS-164808	145.2	Moss, unidentifiable	2.4	-26.8	0.2169	0.0019	12,300	70	14,750 15,050	44%
UCIAMS-239748	181.0-182.5	<i>Drepanocladus</i> , <i>Paludella squarrosa</i> , <i>Potamogeton</i> , unidentifiable	6.8	-19.4	0.1949	0.0006	13,135	30	<sup>a</sup> 19,350 19,600	100%
UCIAMS-239746	185.5-188.5	Moss, <i>Potamogeton</i> , unidentifiable	2.1	-14.6	0.1875	0.0006	13,450	25	14,050 14,550	84%
UCIAMS-239745	239.0-241.5	Unidentifiable	2.5	NA	0.1910	0.0009	13,300	40	14,700 14,850	16%
OS-162874	255.0	Moss, unidentifiable	2.5	-26.6	0.2029	0.0020	12,800	80	<sup>a</sup> 15,650 15,900	100%
<b>Vincent-3 (20VIN3)</b>										
UCIAMS-239753	34.5-35.5	<i>Chara</i> , unidentifiable	25.8	-15.3	0.1988	0.0006	12,980	25	<sup>a</sup> 16,050 16,300	100%
OS-162873	146.5-152.0	Unidentifiable	2.1	-26.6	0.2100	0.0020	12,550	75	15,800 16,150	100%
<b>Vincent-4 (20VIN4)</b>										
UCIAMS-239752	17.0-18.0	Beetle wing, <i>Gladocera</i> , <i>Chara</i> , unidentifiable	5.1	-24.9	0.2126	0.0007	12,435	30	15,050 15,550	100%
UCIAMS-239751	87.0-88.0	Unidentifiable	39.2	NA	0.2127	0.0010	12,435	40	<sup>a</sup> 15,350 15,650	100%
UCIAMS-239750	97.5-98.8	Unidentifiable	6.3	NA	0.2150	0.0011	12,350	45	14,300 14,900	100%
									14,150 14,550	76%
									14,700 14,850	24%

continued

OS-162875	174.0-175.0	Twig	2.0	-28.0	0.2120	0.0019	12,450	75	14,250	15,000	100%
<b>Songster (21SONG1)</b>											
OS-160884	39.3	Bark (likely <i>Picea</i> )	6.4	NA	0.2107	0.0015	12,500	55	14,350	14,750	55%
							14,750		14,750	15,050	45%
<b>Allenberg (15ABB7)</b>											
OS-123347	971.0	Not identified	NA	-26.0	0.8877	0.0019	955	20	795	875	79%
									895	920	19%
OS-123426	1178.0	Not identified	NA	-27.1	0.4580	0.0018	6,270	30	7,160	7,270	96%
OS-123427	1295.0	Not identified	NA	-26.8	0.2607	0.0020	10,800	60	12,700	12,850	100%
OS-123348	1456.0	Not identified	NA	-24.6	0.2227	0.0012	12,050	40	13,800	14,050	100%
<b>Little Protection (21LPB1)</b>											
OS-163424	53.7	Wood	4.6	-24.6	0.5464	0.0014	4,860	20	5,580	5,600	89%
									5,640	5,650	6%
OS-163425	141.0	Wood	15.6	-28.3	0.4549	0.0017	6,330	30	7,170	7,220	44%
OS-163426	198.5	Wood	39.7	-28.0	0.4376	0.0013	6,640	25	7,240	7,320	56%
OS-163427	320.5	<i>Potamogeton</i>	5.4	-17.6	0.3295	0.0012	8,920	30	<sup>a</sup> 9,910	10,100	66%
									10,100	10,200	34%
OS-163428	423.0	Seed pod	5.8	-28.0	0.3034	0.0015	9,580	40	10,750	11,100	99%
OS-163517	472.2	<i>Picea</i> cone	5.5	-25.7	0.2512	0.0016	11,100	50	12,900	13,100	100%
OS-163500	481.0	Wood	32.9	-27.0	0.2346	0.0017	11,650	60	13,350	13,600	100%
OS-163501	493.0	Wood	3.0	-27.3	0.2277	0.0015	11,900	55	13,600	13,850	89%
									13,950	14,000	11%
OS-163429	511.0	Fish bone	11.0	-26.5	0.1749	0.0023	14,000	110	<sup>a</sup> 16,650	17,350	100%
<b>Dragonfly (13DFK1)</b>											
OS-106743	25.2	Twig	NA	-22.8	0.6025	0.0031	4,070	40	4,420	4,650	82%
									4,760	4,800	13%
OS-106745	194.9	Moss stems	NA	-26.6	0.3381	0.0016	8,710	40	9,550	9,780	95%
OS-106746	362.4	Moss stems	NA	-25.0	0.3157	0.0017	9,260	45	10,300	10,550	100%
OS-133658	431.5	Leaf	NA	-25.7	0.2729	0.0015	10,450	45	12,100	12,400	55%
									12,400	12,500	19%
OS-106747	453.5	Twig	NA	-25.9	0.2704	0.0017	10,500	50	12,550	12,600	26%
									12,200	12,250	5%

continued

OS-133659	482.5	Wood	NA	-25.6	0.2447	0.0016	11,300	50	12,250	12,300	6%
OS-106863	524.6	Twig	NA	-25.3	0.2428	0.0011	11,350	35	12,300	12,350	4%
OS-133660	541.6	Twig	NA	-25.7	0.2220	0.0015	12,100	55	12,450	12,700	84%
OS-107085	567.6	Grass	NA	-35.4	0.2048	0.0014	12,750	55	13,100	13,250	88%
									13,250	13,300	12%
									13,150	13,300	100%
									13,800	14,100	100%
									15,000	15,400	100%

<sup>a</sup> Samples not used in the discussion due to possible hardwater effect

NA: Not Available.

NA  $\delta^{13}\text{C}$ : Sample was either too small or the measurement was not requested.

NA Mass: Not recorded

365

#### 366 4.2.3 Optically stimulated luminescence dating

367 Our small-aliquot  $D_e$  results from both 21SICK-01 and -02 show evidence of partial bleaching, as expected  
368 in a glaciofluvial environment (Table 3; AFig. 1 & 2; Rittenour et al., 2015).  $D_e$  results from the two samples are  
369 considerably scattered, positively skewed, and have overdispersion values between ~30 and ~60%, all indicative of  
370 incomplete bleaching and justify the use of the MAM (e.g., Olley et al. (1999)). Our two OSL MAM ages are  $19.8 \pm$   
371  $2.6$  and  $20.6 \pm 2.9$  ka. The two samples are from within 10 cm of each other and yield statistically indistinguishable  
372 ages.

Table 3. Optically Stimulated Luminescence Age Information

Sample num.	USU num.	Depth (m)	Num. of Analyses <sup>1</sup>	Dose Rate (Gy/kyr)	Equivalent Dose <sup>2</sup> $\pm 2\sigma$ (Gy)	OSL Age $\pm 1\sigma$ (ka)
21-SICK-1	USU-3622	2.05	21 (42)	$2.70 \pm 0.11$	$53.55 \pm 11.51$	$19.82 \pm 2.60$
21-SICK-2	USU-3623	2.15	23 (37)	$2.23 \pm 0.09$	$46.09 \pm 10.07$	$20.63 \pm 2.91$

<sup>1</sup> Age analysis using the single-aliquot regenerative-dose procedure of Murray and Wintle (2000) on 0.4-1-mm small-aliquots (SA) of quartz sand (150-250  $\mu\text{m}$ ). Number of aliquots used in age calculation and number of aliquots in parentheses.

<sup>2</sup> Equivalent dose ( $D_e$ ) calculated using the Minimum Age Model (MAM) of Galbraith and Roberts (2012).

373

374

## 375 5 Discussion

### 376 5.1 Stratigraphy

377 We interpret Unit 1 as the primary till that comprises the Kent Moraine. At the Vincent-1 (20VIN1) site we  
378 cored from 4.1 to 6.6 m below the wetland surface (2.5 m), but only recovered 1.2 m due to compaction with the  
379 GeoProbe system. We assume we reached below the post-glacial infill and into the primary glacial deposit since this  
380 unit spans 2.5 m and we found no changes in stratigraphy (Fig. 5).

381 Given the hummocky nature of the moraines (Fig. 3), and the complex stratigraphy within Unit 2 (Fig. 5),  
382 and the similarity between Unit 2 from all sediment cores, we interpret this unit to record the transition from an  
383 ice-cored moraine to the modern kettled topography for both moraines. The most striking feature of Unit 2 ~~is~~  
384 ~~sediment cores~~ are the numerous transitions between fine- and coarse-grained deposition. We interpret Unit 2 silt  
385 and clay as being settled out of suspension in lacustrine conditions, indicating that all seven basins likely held small  
386 kettle lakes of shifting dimension during this period. We propose that the alternating clay and diamicton sediments  
387 captured in 20VIN4, on the Kent Moraine, are slumps of primary till into the kettle lake with otherwise clay-rich  
388 sedimentation; these slumps ~~potentially probably~~ occurred as buried glacial ice melted and destabilized the basin's  
389 slopes. The stratigraphy of Unit 2 in ~~from~~ 21LPB1, on the Lake Escarpment Moraine, is likely the result of similar  
390 processes. ~~the changing depositional environments on the moraine as the kettle formed. Higher energy deposits of~~  
391 ~~sand and gravel at the base of the unit were likely deposited atop the ice-cored moraine in fluvial or shallow water~~

~~392 settings before being redeposited, in stratigraphic position, by the melting of buried ice beneath them. These  
393 sediments then floored the new kettle lake and deposition of lacustrine silt began.~~

394 The transition in sediment type between Units 2 and 3 likely reflects a shift to a more vegetation growing in  
395 the lake productive lake and landscape, in concert with increased stabilization of the surrounding moraine. ~~Some~~  
396 layers of minerogenic sediment in the bottom of Unit 3 in 20VIN1 & 20VIN3 show that the landscape continued to  
397 receive sediment from primary glacial deposits after the transition to more organic-rich deposition. We infer the  
398 minerogenic sediments in the transition zone ~~that the~~ (inclusions of gray clay and brown silty macrofossils in  
399 20VIN1) are rip-up clasts by their clast-like appearance and stark contrast to the surrounding sediment (Fig 5; Panel  
400 C). They were potentially frozen during the time of deposition. This ~~further~~ suggests the presence of reworked  
401 material near the Unit 2/3 transition. The subsequent transition from lacustrine organic-rich silt to peat (Lower and  
402 Upper Unit 3, respectively) records the shift from lake to bog/wetland due to the filling of the basin, shallowing of  
403 the lake, and encroachment of the shoreline.

404

## 405 5.2 Chronology

406 ~~The OSL ages support our estimated age of 25 – 20 ka for the Kent Moraine from prior literature and  
407 affirms our confidence in the age assignments using correlations of dated features elsewhere.~~ The OSL samples are  
408 from 2 m below the surface of the ~70 m thick kame delta. The sample location within the topset beds of a  
409 short-lived ice-contact delta suggests that our OSL samples constrain the time just before the ice sheet retreated and  
410 ceased building the delta  $19.8 \pm 2.6 - 20.6 \pm 2.9$  ka. The OSL ages support the estimated age of 25 – 20 ka for the  
411 Kent Moraine from prior literature and affirms our confidence in the age assignments using correlations of dated  
412 features elsewhere (Balco et al., 2009; Balco et al., 2002; Corbett et al., 2017; Glover et al., 2011; Stanford et al.,  
413 2020).¶

414 ~~The basal ages, taken at face value, indicate the deposition of the Kent Moraine occurred prior to shortly  
415 before 15 ka; this does not agree with our OSL age or the regional correlations. Furthermore, a Kent Moraine age  
416 of 15 ka contradicts the 17 ka age for the Lake Escarpment Moraine, which lies up ice flow from the Kent  
417 Moraine. The above information, combined with our evidence for an unstable landscape depicted from our sediment  
418 core stratigraphy and numerous age reversals, suggests that our radiocarbon ages from Unit 2 consist of organic  
419 material that was reworked into these kettles during kettle formation.~~

420 We have identified spores and seeds of aquatic plants *Chara* and *Potamogeton* (O. Bennike, personal  
421 communication) among the macrofossils from samples dating to 15,800 - 16,150, 16,050-16,300 and 15,650-15,900  
422 cal yr BP from 20VIN1 and the sample dating to 15,350-16,650 cal yr BP from 20VIN3. These macrofossil samples  
423 also have enriched  $\delta^{13}\text{C}$  values, suggesting they ~~at these samples~~ contained aquatic material (except 15,800 - 16,150,  
424 which was too small for a  $\delta^{13}\text{C}$  measurement; Deuser and Degens, 1967; Oana and Deevey, 1960; Wang and  
425 Wooller, 2006). Our sites lie within calcareous tills that overlie sedimentary bedrock (LaFleur, 1979; MacClintock  
426 and Apfel, 1944), which can add aged carbon to the lake water. Aquatic plants derive their carbon from lake water,  
427 so radiocarbon ages from aquatic plants could produce radiocarbon ages that overestimate the age of the material

428 (the 'hardwater effect'; Deevey et al., 1954; Keeley and Sandquist, 1992). The lowest sample in 21LPB1 is from a  
429 fish bone (16,650 - 17,350 cal BP); a fish could be susceptible to the same hardwater effect as aquatic vegetation,  
430 and thus we do not use it in our evaluation. We move forward using samples assumed to be terrestrial from a lack of  
431 identifiable aquatic macrofossils and supported by  $\delta^{13}\text{C}$  values. ¶

432 ~~We move forward using samples assumed to be terrestrial from a lack of identifiable aquatic macrofossils~~  
433 ~~visual identification and supported by  $\delta^{13}\text{C}$  values. Four ages from 20VIN1 Unit 2 remain: 19,350-19,600,~~  
434 ~~15,050-15,550, 14,300-15,050, and 14,050-14,850 cal yr BP. We limit the 20VIN3 chronology to one trustworthy~~  
435 ~~age of 14,350-15,150 cal yr BP from Unit 2. We derived the age of 16,650-17,350 cal yr BP in 21LPB1 from a fish~~  
436 ~~bone; a fish could be susceptible to the same hardwater effect as aquatic vegetation, and thus we do not use it in our~~  
437 ~~evaluation. Instead, we use the next lowest age of 13,600-14,000 cal yr BP as the basal age, along with~~  
438 ~~15,000-15,400 cal yr BP from 13DFK1.~~

439 The Unit 2 ages are trustworthy as minimum-limiting constraints on moraine abandonment, but we find the  
440 evidence for slumps and rip-up clasts in Unit 2, plus the stratigraphic discordance in radiocarbon ages, reason to  
441 doubt the reliability of the radiocarbon ages to reflect the age of the sediment they are within. ~~These age estimates~~  
442 ~~that are assumed to be more trustworthy still exhibit age reversals. These ages support our interpretation from the~~  
443 ~~visual stratigraphy that reworked sediments contain organic matter that does not accurately date to the sediment's~~  
444 ~~deposition. The~~ Our oldest minimum-limiting constraint from Unit 2 is from the macrofossil-rich rip-up clast in  
445 20VIN1 on the Kent Moraine, which holds evidence for two important interpretations: 1) the landscape was ice-free  
446 and at least sparsely vegetated as early as 19,350-19,600 cal yr BP, (consistent with our OSL ages suggesting ice  
447 sheet retreat by  $19.8 \pm 2.6 - 20.6 \pm 2.9$  ka), and 2) the landscape stored this long-dead vegetation for thousands of  
448 years before it was re-deposited. This age also bolsters our confidence that the MAM is working well in our study  
449 area.

450 We use the lowest ages in Unit 3 as minimum-limits on the timing of kettle formation and moraine  
451 stabilization. The lowest ages from Unit 3 from the Kent Moraine range from 13,650 - 14,050 (20VIN1) to 14,350 -  
452 15,050 (21SONG1) cal BP. The lowest ages from Unit 3 from the Lake Escarpment Moraine are 13,600 - 14,000  
453 (21LPB1) to 15,000 - 15,400 (13DFK1) cal BP. The range of ages shows the kettles formed through the interval of  
454 13,600 to 15,400 cal BP, reflecting the time the moraines stabilized. This shows both moraines stabilized at the same  
455 time, even though they are likely several thousands years different in age. Using our OSL ages and  
456 minimum-limiting radiocarbon age from Unit 2 to estimate the deposition of the Kent Moraine before 19,350 -  
457 19,600 cal yr BP, there appears to be a 5 kyr lag time between moraine deposition and stabilization.

458 ~~Since we do not trust that radiocarbon ages from Unit 2 accurately date the time of sediment deposition,~~  
459 ~~and the moraine ages are incompatible with regional correlations, we do~~ ~~Since we do not interpret our lowest, basal~~  
460 ~~ages to record the timing of ice recession and abandonment of the moraines. Instead, we interpret these younger than~~  
461 ~~expected ages to record kettle basin formation and moraine stabilization for both the Kent and Lake Escarpment~~  
462 ~~moraines between 15,000-15,4000 and 13,600-14,000 cal yr BP. This interpretation also reconciles the similar basal~~  
463 ~~ages between both moraines that are likely several thousand years different in age. ¶~~

464

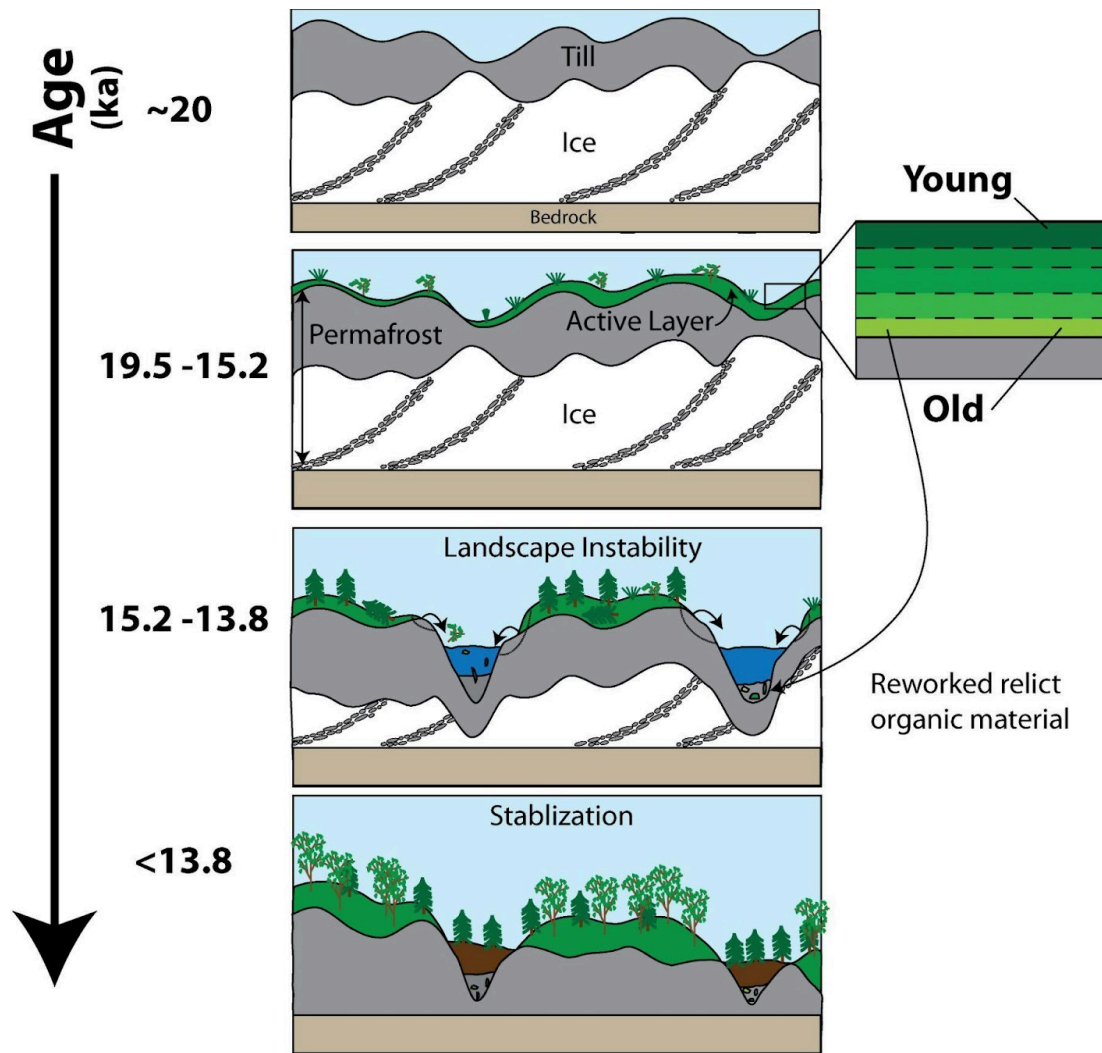
### 465 5.3 A model for kettle basin formation

466 We propose the following post-glacial history in western New York (Fig. 6). The deposition of the Kent  
467 Moraine occurred at least  $19.8 \pm 2.6 - 20.6 \pm 2.9$  ka and the landform remained ice-cored for the ensuing 5 – 6 kyr.  
468 The deposition of the Lake Escarpment Moraine took place around 17 ka and likewise remained ice-cored for the  
469 next 2 – 3 kyr. The hummocky nature of the moraines indicate that they were ice-cored, and we suggest that  
470 persistent buried glacial ice prohibited stabilization until well after deposition. Our interpretation is that after ~15 ka  
471 buried ice began to melt, and morainal topography – including kettle basins – began to evolve more rapidly (Fig. 6  
472 & 7). During the earliest stages of kettle basin formation, there was increased mobilization of sediments from within  
473 the uneven ice-rich topography. These initial sediments contained both re-worked and contemporary organic matter  
474 from the catchment and were deposited in our study sites as Unit 2. According to this interpretation, our radiocarbon  
475 ages from Unit 2 could reflect plant death anytime between moraine deposition and kettle basin stabilization. The  
476 13,750 - 15,250 cal BP wood age from basal lake sediments in Nichols Brook is likely another example of delayed  
477 kettle formation in this area (Fritz et al., 1987). ~~do not record the initial deposition of these moraines, but instead its~~  
478 ~~stabilization ~15 to 14 ka.~~

479 ~~Ice-cored m~~Moraines can remain ice-cored for thousands of years after deposition due to sediment cover  
480 that insulates and preserves the buried ice (Florin and Wright, 1969). If the region is cold enough to support  
481 permafrost it may extend the duration that the moraine remains ice-cored (Clayton et al., 2001; Henriksen et al.,  
482 2003; Schomacker, 2008). Given that the kettles appear to have formed within ~1 kyr of each other, and their  
483 formation coincided with the warm Bølling/Allerød period, this suggests the climate during Heinrich Stadial 1 may  
484 have been cold enough to help preserve the ice.

485





486

487 Figure 6. Conceptual model of kettle basin formation of the Kent Moraine in western New York building on Florin and  
 488 Wright (1969). The same model applies to the Lake Escarpment moraine, except the timeline begins ~17 ka. First, the LIS  
 489 deposited the ice-cored Kent Moraine. It remained ice-cored, perhaps influenced by permafrost, while tundra vegetation  
 490 grew atop the moraine and stored carbon in the soil. Next, during climate amelioration in the Bølling-Allerød periods, the  
 491 ice in the moraine melted. This led to the formation of basins that filled with both contemporaneous and reworked  
 492 sediments. This is also likely the time when trees and other organic material could be slumped and formed deposits that  
 493 placed primary tills adjacent to younger material. Finally, organic-rich sediment deposition dominates after ~13.8 ka.

494

#### 495 5.4 Implications for the climate in western New York

496 The climate of western New York between 20 and 15 ka is poorly known, but records from Ontario, Ohio,  
 497 and New England suggest the climate events of the North Atlantic influenced the northeastern U.S. These terrestrial  
 498 climate reconstructions depict a cold Heinrich Stadial 1 (~18 to ~14.7 ka), a shift to warmer temperatures during the  
 499 Bølling-Allerød, and a cool Younger Dryas (Gill et al., 2012; Gonzales and Grimm, 2009; Grigg et al., 2021;  
 500 Shuman et al., 2002; Watson et al., 2018; Yu, 2007; Yu and Eicher, 1998). A stable Heinrich Stadial 1 and shift to

501 warmer temperatures during the Bølling-Allerød is shown by Watson et al. (2018), who used biomarkers  
502 (branched-GDGTs) to report that mean annual temperature in central Ohio varied between  $-2.0$  and  $-0.5$  °C from  
503 17.0 to 14.5 ka before warming  $5^{\circ}\text{C}$  between 14.5 and 13.0 ka.

504 The rate of LIS retreat offers additional insight into the climate in the northeast US. Barth et al. (2019) used  
505 cosmogenic nuclide dating of glacially-transported boulders to estimate LIS thinning in the Adirondack Mountains  
506 and showed increased thinning between  $15.4 \pm 1.0$  and  $13.9 \pm 0.9$  ka, generally coincident with the Bølling. The  
507 New England Varve Chronology shows a relatively steady net retreat rate of the LIS through the Hudson Valley  
508 between 18 and 14.7 ka; during the Bølling the net retreat rate tripled, implying that New England experienced  
509 elevated warmth at that time (Ridge et al., 2012).

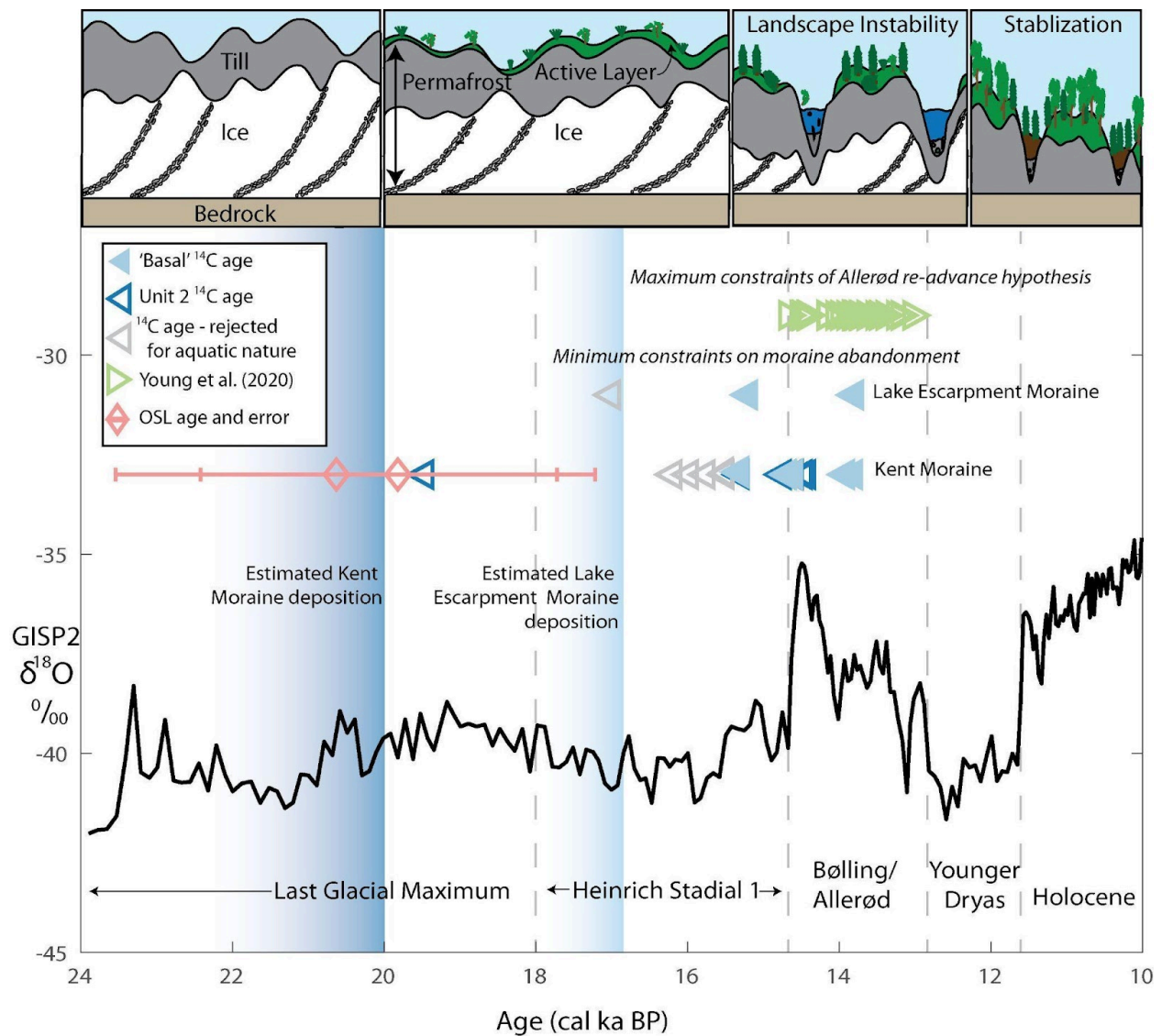
510 Ice-wedge casts can be used to identify areas that experienced past permafrost and constrain past  
511 temperature because their formation requires mean annual temperatures between  $-6$  to  $-8^{\circ}\text{C}$  (French, 2007; French  
512 and Miller, 2014). Ice-wedge casts are preserved in southern Ontario that were deposited 18-15 ka based on regional  
513 correlations (Dalton et al., 2020; Gao, 2005; Morgan et al., 1982). This suggests that the mean annual air  
514 temperature was low enough near our study site during Heinrich Stadial 1 to support permafrost. While this  
515 temperature depression is larger than reported by Watson et al. (2018), it's likely there was a strong temperature  
516 gradient between Ohio and western New York during deglaciation, with the latter remaining within 100 km of the  
517 ice margin until 14 ka (Dalton et al., 2020). This proximity to the ice sheet from the LGM to 14 ka may have been a  
518 driver of the cold climate that persisted in western New York. There are no reports of relict permafrost features  
519 within the LGM limit in western New York, but their presence south of the LGM extent suggest the likelihood of  
520 permafrost within the limit as well (French and Millar, 2014).

521 Finally, there are seven local pollen records from Miller (1973), Calkin and McAndrews (1980), and Doody  
522 (2018) that describe the initial deglacial vegetation in western New York. Only the Allenberg Bog (Miller, 1973) and  
523 Dragonfly Kettle (Doody, 2018) pollen records captured a ‘tundra’ zone at the base, although the presence of both  
524 arctic and temperate vegetation complicates their interpretation. ~~The tundra zone is overlain by an interval with high~~  
525 ~~spruce and pine pollen; this is the lowest unit found in the other five records (Miller, 1973; Calkin and McAndrews,~~  
526 ~~1980). This is likely reflecting the new forest biome associated with warmer temperatures.~~ Given our results, we  
527 believe ~~this~~ ‘tundra’ pollen ~~tundra~~ zone captured both the tundra vegetation that was growing on the moraine prior  
528 to basin formation and the more temperate vegetation as spruce and pine moved in during the Bølling.  
529 Unfortunately, the pollen records may be unreliable before 14 ka due to the same reworking problems as our  
530 radiocarbon dating, but this remains site specific. ~~The tundra zone is overlain by an interval with high spruce and~~  
531 ~~pine pollen; this is the lowest unit found in the other five records (Miller, 1973; Calkin and McAndrews, 1980). This~~  
532 ~~is likely reflecting the new forest biome associated with warmer temperatures.~~

533 Altogether, there is evidence that the lag time between ice sheet retreat and kettle basin stabilization may be  
534 attributable to sustained permafrost in western New York due to cold North Atlantic conditions during Heinrich  
535 Stadial 1 (Fig. 7). The warming at the Bølling onset at  $\sim 14.7$  ka may have increased regional temperatures, causing  
536 the melting of buried ice, initiating a phase of rapid landscape evolution and the formation of kettle basins, and  
537 eventually stabilizing the morainal topography. Numerous studies discuss the role of permafrost in the lag time

538 between moraine ages and basal macrofossils along the south-central LIS margin, including Indiana and Illinois  
 539 (Curry et al., 2018; Fisher et al., 2020), Michigan (Yansa et al., 2020), and Wisconsin (Clayton et al., 2008).

540 Our findings support the observations and conclusions from numerous studies that radiocarbon dates can be  
 541 extreme minimum age constraints on deglaciation (Curry et al., 2018; Fisher et al., 2020; Florin and Wright, 1969;  
 542 Halsted et al., 2023; Yansa et al., 2020). In New England, minimum-limiting radiocarbon ages may be the reason for  
 543 the discrepancy between the timing of moraine deposition as recorded by  $^{10}\text{Be}$  exposure dating (e.g., Balco et al.,  
 544 2002; Corbett et al., 2017) and radiocarbon ages of basal macrofossils in lakes and bogs (e.g., Peteet et al., 2012).  
 545 The younger than expected radiocarbon ages from the Valley Heads Moraine from Kozłowski et al. (2018) may be  
 546 afflicted by similar processes. Permafrost during Heinrich Stadial 1 may have minimized landscape evolution in  
 547 New England and central New York as well and could help explain the offset.



548

549 Figure 7. Comparison of radiocarbon ages from the Kent and Lake Escarpment moraine and Young et al. (2020) in the  
 550 context of North Atlantic deglacial climate changes. Black line is the GISP2  $\delta^{18}\text{O}$  record (Grootes and Stuiver, 1999). Dark  
 551 blue and light blue fading is the estimated deposition of the Kent Moraine and Lake Escarpment Moraine, respectively.

552 Dark blue and light blue triangles are the lowest reliable radiocarbon ages from the Kent and Lake Escarpment Moraine  
553 sediment cores, respectively. Gray triangles are radiocarbon ages that we suspect have hardwater contamination. Pink  
554 diamonds are OSL ages and  $2\sigma$  errors from the kame delta outboard the Kent Moraine. Green triangles are ages from  
555 Young et al. (2020) interpreted by them to be maximum-limiting constraints on the 13 ka re-advance. Errors for all  
556 radiocarbon dates are not plotted because their width is smaller than the symbols.

557

## 558 5.5 Allerød re-advance hypothesis

559 The stratigraphically lowest radiocarbon ages from Unit 3 in the Lake Escarpment Moraine kettle basins,  
560 which are 15,000-15,400 and 13,600-14,000 cal ~~yr~~BP, pre-date the ~13.1 ka re-advance suggested by Young et al.  
561 (2020) (Fig. 5 & 7). Chronologically constrained organic-rich sedimentation, with no stratigraphic evidence of  
562 interruption, ensued from at least 13,600-14,000 cal ~~yr~~BP and well into the Holocene. Furthermore, there is no  
563 evidence of over-compaction in our bulk density measurements in 21LPB1 during this interval of time (Fig. 5).  
564 Thus, we do not find evidence that a ~13.1 ka LIS advance created or overran the Lake Escarpment Moraine as  
565 hypothesized by Young et al. (2020). Rather, we suggest that the landscape was unstable during its transition from a  
566 permafrost-dominated landscape to one with evolving and then stabilizing morainal topography. This landscape  
567 instability with reworking of glacial sediments may have led to the stratigraphy interpreted by Young et al. (2020) as  
568 primary tills in contact with ~~logstrees~~ dating to 13 ka (Fig. 7). Both the Dragonfly and Little Protection sites have  
569 intervals with increased wood deposition between 14 and 13 ka and future work could investigate the source of these  
570 woody intervals to further investigate the results from Young et al. (2020).

571

## 572 6 Conclusion

573 We present 41 new macrofossil-based radiocarbon ages from kettle basin infills in western New York. We  
574 find that the lowest ~~reliable~~ radiocarbon ages ~~from Unit 3-between~~ (15,000-15,400 and 13,600-14,000 cal ~~yr~~BP) are  
575 ~~2–56 kyr~~ younger than our OSL age constraints on moraine deposition of  $19.8 \pm 2.6 - 20.6 \pm 2.9$  ka and the oldest  
576 radiocarbon age from Unit 2 of 19,350-19,600 cal BP from the Kent Moraine. These lowest Unit 3 ages are 2 kyr  
577 younger than our estimated age of Lake Escarpment Moraine deposition from moraine correlations. We interpret this  
578 offset to be due to a cold climate in western New York during Heinrich Stadial 1 supporting persistent buried ice  
579 which inhibited kettle basin formation until regional warming that took place during the Bølling. Our results do not  
580 support a re-advance of the LIS over the Lake Escarpment Moraine ~13 ka (c.f. Young et al., 2020). The lag time  
581 between ice sheet retreat and moraine stabilization in western New York may present an alternate explanation for  
582 inconsistencies between basal ages in sediment cores and other dating methods in central New York (Kozłowski et  
583 al., 2018) and eastern New York (Petet et al., 2012).

584 Future work could target features that are stable during ice retreat even where permafrost is present, such as  
585 outcrops of pro-glacial and ice-walled lake plane deposits (e.g., Curry et al., 2018), or perhaps moraines that are not  
586 hummocky in nature. This limitation may not be as necessary in environments where climate more quickly  
587 ameliorated, such as appears to have been the case in southern Ohio (Glover et al., 2011). Additionally, it may be  
588 important to consider the coring equipment. The GeoProbe coring device enabled us to collect stiff mineral-rich

589 sediments lower than otherwise possible with the Livingstone and Russian Peat coring devices. This meant that our  
 590 coring did not stop at first contact with stiff minerogenic sediment that could mistakenly be interpreted as primary  
 591 glacial in origin.

592

593 **Appendix A.**

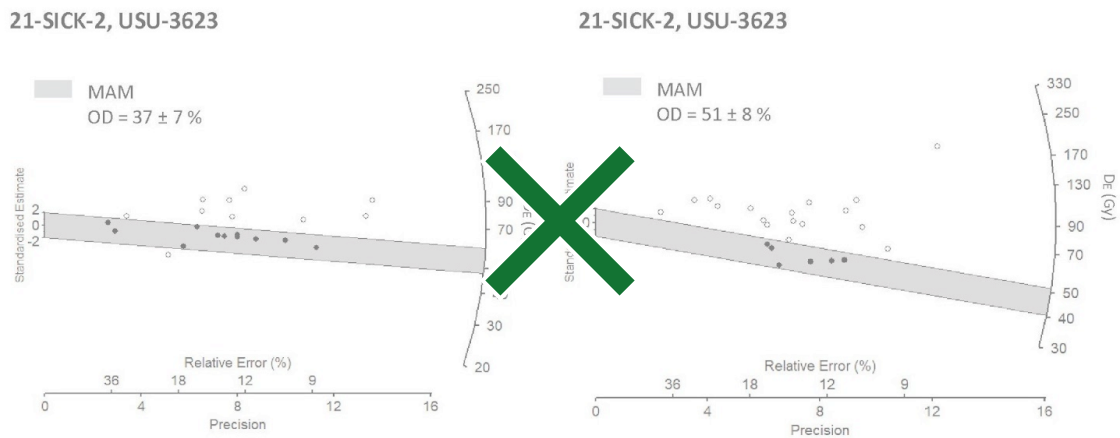
Table A1: Dose Rate Information

USU num.	Lat/Long	In-situ H <sub>2</sub> O (%)	D <sub>R</sub> Subsample <sup>1</sup>	K (%) <sup>2</sup>	Rb (ppm) <sup>2</sup>	Th (ppm) <sup>2</sup>	U (ppm) <sup>2</sup>	Cosmic (Gy/kyr)
USU-3622	42.11394/ -78.94899	7.5	F: 70%	1.64±0.04	77.6±3.1	7.8±0.7	2.6±0.2	0.18±0.02
			M: 20%	1.2±0.03	58.7±2.3	8.6±0.8	2.2±0.2	
			C: 10%	1.1±0.03	76.1±3.0	11.1±1.0	2.1±0.1	
USU-3623	42.11394/ -78.94899	20.0	F: 85%	1.2±0.03	74.4±3.0	8.3±0.7	2.0±0.1	0.18±0.02
			M: 15%	1.35±0.03	72.7±2.9	8.4±0.8	2.4±0.2	

<sup>1</sup> Dose rate (D<sub>R</sub>) subsamples based on grain size: fine-F (<1.7 mm), medium-M (1.7-16 mm), coarse-C (>16 mm), and weighted proportions (%) of subsamples used with chemistry in gamma dose rate calculation. Beta dose rate uses chemistry from fine fraction (<1.7 mm) only.

<sup>2</sup> Radioelemental concentrations determined using ICP-MS and ICP-AES techniques; dose rate is derived from concentrations by conversion factors from Guérin et al. (2011).

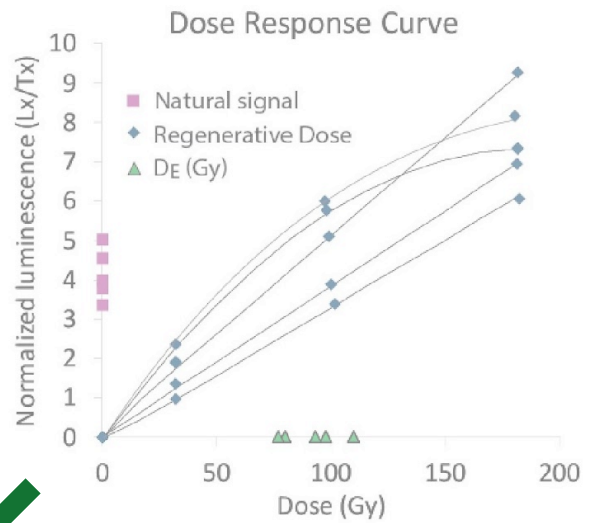
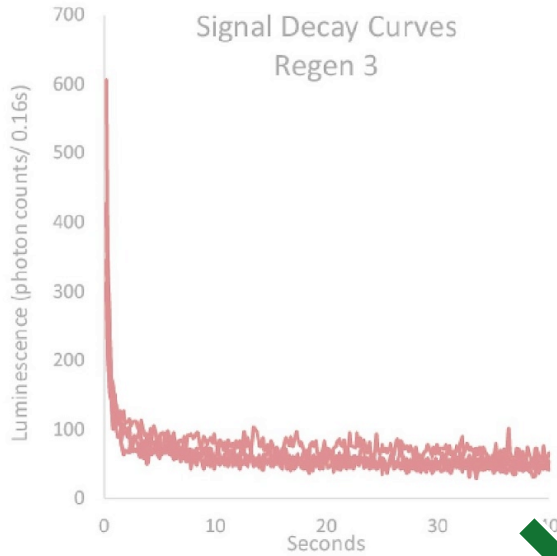
594



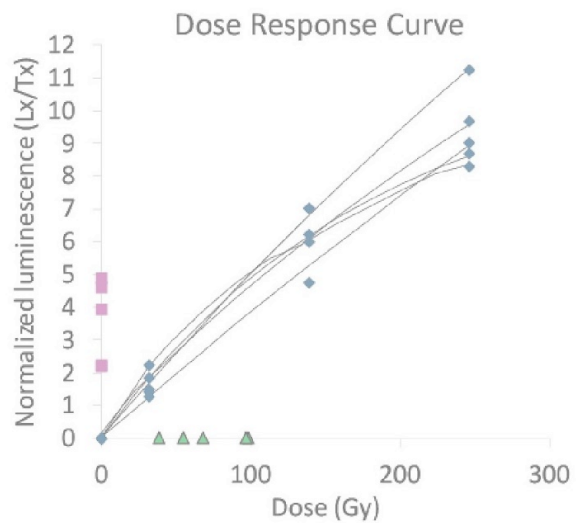
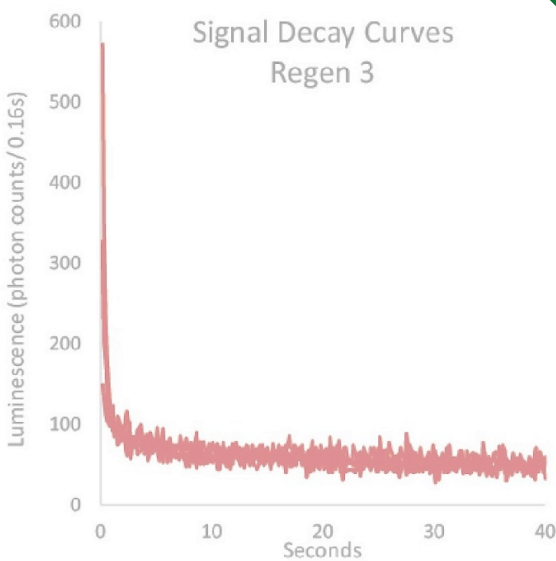
595

596 ~~Figure A1. Equivalent dose ( $D_e$ ) distributions for the luminescence samples collected from the kame delta associated with~~  
 597 ~~an ice margin position near the Kent moraine. MAM = minimum age model of Galbraith and Roberts (2012) fit to the  $D_e$~~   
 598 ~~data (gray shaded region). OD = overdispersion, a metric of  $D_e$  scatter beyond instrumental error, where  $OD > 30\%$  is~~  
 599 ~~interpreted to be due to partial bleaching due to incomplete solar resetting of the luminescence signals in the quartz~~  
 600 ~~grains.~~

USU-3622



USU-3623



601

602 ~~Figure A2. Example luminescence signal decay (left) and dose-response curves from 5 aliquots from each of the~~  
603 ~~luminescence samples.~~

604

605 **Data availability:** Table 2 provides the data to calculate the radiocarbon ages from this study. Table 3 and Table A1  
606 provide the data to calculate OSL ages from this study.

607

608 **Author contributions:** JPB and KKP conceptualized the study. ALK and KKP provided funding for fieldwork and  
609 lab analyses. KKP, JPB, CKW, BMC, and EPY collected sediment cores. KKP, BMC, EPY and JPB conducted

610 downcore analyses and radiocarbon sampling. CKW collected OSL samples and TMR conducted lab analyses and  
611 calculated the ages. KKP compiled and recalculated the radiocarbon ages. KKP, JPB, ALK, CKW, and BMC  
612 interpreted the results. KKP wrote the first draft of the manuscript and all authors contributed to editing. KKP and  
613 TMR developed the figures and tables.

614

615 **Competing interests.** The authors declare that they have no conflict of interest.

616

617 **Acknowledgements:** We thank the Vincent, Songster, Gebhard, and Bohall families for the access to their property,  
618 as well as their enthusiasm and friendship. We thank Joseph Tulenko, Brandon Graham, Elizabeth Thomas, Kurt  
619 Lindberg, Owen Cowling, Fiona Ellsworth, Joshua Charlton, Liza Wilson, Jason Parsons, Will Phillips, and George  
620 Thomas for their help in the field (it takes a village!). We thank the National Ocean Sciences Accelerator Mass  
621 Spectrometry and W. M. Keck Carbon Cycle Accelerator Mass Spectrometer laboratories for radiocarbon analyses.  
622 We thank the Luminescence Lab at Utah State University for OSL analyses.

623

624 **Funding sources:** This research was supported by the United State Geological Survey Great Lakes Geological  
625 Mapping Coalition grant #G20AC00418, the NSF/GSA Graduate Student Geoscience grant # 13056-21, which was  
626 funded by NSF Award # 1949901, and the Mark Diamond Research Fund of the Graduate Student Association of  
627 the State University of New York at Buffalo.

628

## 629 **References**

630 Balco, G., Stone, J. O. H., Porter, S. C., and Caffee, M. W.: Cosmogenic-nuclide ages for New England coastal  
631 moraines, Martha's Vineyard and Cape Cod, Massachusetts, USA, *Quaternary Science Reviews*, 21, 2127–2135,  
632 [https://doi.org/10.1016/S0277-3791\(02\)00085-9](https://doi.org/10.1016/S0277-3791(02)00085-9), 2002.

633 Balco, G., Briner, J., Finkel, R. C., Rayburn, J. A., Ridge, C., and Schaefer, J. M.: Regional beryllium-10 production  
634 rate calibration for late-glacial northeastern North America, *Quaternary Geochronology*, 4, 93-107,  
635 <https://doi.org/10.1016/j.quageo.2008.09.001>, 2009.

636 Barth, A. M., Marcott, S. A., Licciardi, J. M., and Shakun, J. D.: Deglacial Thinning of the Laurentide Ice Sheet in  
637 the Adirondack Mountains, New York, USA, Revealed by <sup>36</sup>Cl Exposure Dating, *Paleoceanography and*  
638 *Paleoclimatology*, 34, 946-953, <https://doi.org/10.1029/2018PA003477>, 2019.

639 Bird, B. and Kozlowski, A.: Late Quaternary Reconstruction of Lake Iroquois in the Ontario Basin of New York.  
640 New York State Museum Map & Chart 80, [https://www.nysm.nysed.gov/sites/default/files/mc80\\_iroquois.pdf](https://www.nysm.nysed.gov/sites/default/files/mc80_iroquois.pdf),  
641 2016.

642 Briner, J. P., Cuzzone, J. K., Badgeley, J. A., Young, N. E., Steig, E. J., Morlighem, M., Schlegel, N. J., Hakim, G.  
643 J., Schaefer, J. M., Johnson, J. V., Lesnek, A. J., Thomas, E. K., Allan, E., Bennike, O., Cluett, A. A., Csatho, B., de

644 Vernal, A., Downs, J., Larour, E., and Nowicki, S.: Rate of mass loss from the Greenland Ice Sheet will exceed  
645 Holocene values this century, *Nature*, 586, 70-74, <https://doi.org/10.1038/s41586-020-2742-6>, 2020.

646 Broecker, W. S., Kennett, J. P., Flower, B. P., Teller, J. T., Trumbore, S., Bonani, G., and Wolfli, W.: Routing of  
647 meltwater from the Laurentide Ice Sheet during the Younger Dryas cold episode, *Nature*, 341, 318-321,  
648 <https://doi.org/10.1038/341318a0>, 1989.

649 Calkin, P. E. and Feenstra, B. H.: Evolution of the Erie-Basin Great Lakes, in: *Quaternary Evolution of the Great  
650 Lakes*, edited by: Karrow, P. F., and Calkin, P. E., Geological Society of Canada,  
651 [https://doi.org/10.1016/0033-5894\(87\)90011-1](https://doi.org/10.1016/0033-5894(87)90011-1), 1985.

652 Calkin, P. E. and McAndrews, J. H.: Geology and paleontology of two late Wisconsin sites in western New York  
653 State, *Geological Society of America Bulletin*, 91, 295-306,  
654 [https://doi.org/10.1130/0016-7606\(1980\)91<295:GAPOTL>2.0.CO;2](https://doi.org/10.1130/0016-7606(1980)91<295:GAPOTL>2.0.CO;2), 1980.

655 Campbell, M. C., Fisher, T. G., and Goble, R. J.: Terrestrial sensitivity to abrupt cooling recorded by aeolian activity  
656 in northwest Ohio, USA, *Quaternary Research*, 75, 411-416, <https://doi.org/10.1016/j.yqres.2011.01.009>, 2011.

657 Clayton, L. E., Attig, J. W., and Mickelson, D. M.: Effects of late Pleistocene permafrost on the landscape of  
658 Wisconsin, USA, *Boreas*, 30, 173-188, <https://doi.org/10.1111/j.1502-3885.2001.tb01221.x>, 2001.

659 Corbett, L. B., Bierman, P. R., Stone, B. D., Caffee, M. W., and Larsen, P. L.: Cosmogenic nuclide age estimate for  
660 Laurentide Ice Sheet recession from the terminal moraine, New Jersey, USA, and constraints on latest Pleistocene  
661 ice sheet history, *Quaternary Research*, 87, 482-498, <https://doi.org/10.1017/qua.2017.11>, 2017.

662 Coulombe, S., Fortier, D., Lacelle, D., Kanevskiy, M., and Shur, Y.: Origin, burial and preservation of late  
663 Pleistocene-age glacier ice in Arctic permafrost (Bylot Island, NU, Canada), *The Cryosphere*, 13, 97-111,  
664 <https://doi.org/10.5194/tc-13-97-2019>, 2019.

665 Cronin, T. M., Rayburn, J. A., Guilbault, J. P., Thunell, R., and Franzi, D. A.: Stable isotope evidence for glacial lake  
666 drainage through the St. Lawrence Estuary, eastern Canada, ~13.1-12.9 ka, *Quaternary International*, 260, 55-65,  
667 <https://doi.org/10.1016/j.quaint.2011.08.041>, 2012.

668 Curry, B. B., Lowell, T. V., Wang, H., and Anderson, A. C.: Revised time-distance diagram for the Lake Michigan  
669 Lobe, Michigan Subepisode, Wisconsin Episode, Illinois, USA, [https://doi.org/10.1130/2018.2530\(04\)](https://doi.org/10.1130/2018.2530(04)), 2018.

670 Dalton, A. S., Margold, M., Stokes, C., Tarasov, L., Dyke, A., Adams, R., Allard, S., Arends, H., Atkinson, N.,  
671 Attig, J., Barnett, P., Barnett, R., Batterson, M., Bernatchez, P., Borns, H., Breckenridge, A., Briner, J., Brouard, E.,  
672 Campbell, J., and Wright, H.: An updated radiocarbon-based ice margin chronology for the last deglaciation of the



- 673 North American Ice Sheet Complex, *Quaternary Science Reviews*, 234, 106223,  
674 <https://doi.org/10.1016/j.quascirev.2020.106223>, 2020.
- 675 Deevey, E. S., Gross, M. S., Hutchinson, G. E., and Kraybill, H. L.: The Natural <sup>14</sup>C Contents of Materials from  
676 Hard-Water Lakes, *Proceedings of the National Academy of Sciences*, 40, 285-288,  
677 <https://doi.org/10.1073/pnas.40.5.285>, 1954.
- 678 Deuser, W. G. and Degens, E. T.: Carbon Isotope Fractionation in the System  
679 CO<sub>2</sub>(gas)—CO<sub>2</sub>(aqueous)—HCO<sub>3</sub><sup>-</sup>(aqueous), *Nature*, 215, 1033-1035, <https://doi.org/10.1038/2151033a0>, 1967.
- 680 Donnelly, J. P., Driscoll, N. W., Uchupi, E., Keigwin, L. D., Schwab, W. C., Thielert, E. R., and Swift, S. A.:  
681 Catastrophic meltwater discharge down the Hudson Valley: A potential trigger for the Intra-Allerød cold period,  
682 *Geology*, 33, <https://doi.org/10.1130/G21043.1>, 2005.
- 683 Doody, E.: A latest pleistocene palynologic record from western New York, *Geology*, University at Buffalo, 2018.
- 684 Dyke, A. S.: An outline of North American deglaciation with emphasis on central and northern Canada, in:  
685 *Developments in Quaternary Sciences*, edited by: Ehlers, J., and Gibbard, P. L., Elsevier, 373-424,  
686 [https://doi.org/10.1016/S1571-0866\(04\)80209-4](https://doi.org/10.1016/S1571-0866(04)80209-4), 2004.
- 687 Elder, K. L., Roberts, M. L., Walther, T., and Xu, L.: Single step Production of graphite from organic Samples for  
688 Radiocarbon Measurements, *Radiocarbon*, 61, 1843-1854, <https://doi.org/10.1017/RDC.2019.136>, 2019.
- 689 Eschman, D. F. and Karrow, P. F.: Huron Basin Glacial Lakes: A Review, in: *Quaternary Evolution of the Great*  
690 *Lakes*, edited by: Karrow, P. F., and Calkin, P. E., Geological Society of Canada,  
691 [https://doi.org/10.1016/0033-5894\(87\)90011-1](https://doi.org/10.1016/0033-5894(87)90011-1), 1985.
- 692 Fairchild, H. L. R.: *Glacial Waters in Central New York*, University of the State of New York 1909.
- 693 Fisher, T. G., Blockland, J. D., Anderson, A., Krantz, D. E., Stierman, D. J., and Goble, R.: Evidence of Sequence  
694 and Age of Ancestral Lake Erie Lake-Levels, Northwest Ohio, *The Ohio Journal of Science* 115,  
695 <https://doi.org/10.18061/ojs.v115i2.4614>, 2015.
- 696 Fisher, T. G., Dziekan, M. R., McDonald, J., Lepper, K., Loope, H., McCarthy, F. M. G., and Curry, B. B.: Minimum  
697 limiting deglacial ages for the out-of-phase Saginaw Lobe of the Laurentide Ice Sheet using optically stimulated  
698 luminescence (OSL) and radiocarbon methods, *Quaternary Research*, 97, 71-87,  
699 <https://doi.org/10.1017/qua.2020.12>, 2020.
- 700 Florin, M.-B. and Wright, H. E., Jr.: Diatom Evidence for the Persistence of Stagnant Glacial Ice in Minnesota, *GSA*  
701 *Bulletin*, 80, 695-704, [https://doi.org/10.1130/0016-7606\(1969\)80\[695:DEFTPO\]2.0.CO;2](https://doi.org/10.1130/0016-7606(1969)80[695:DEFTPO]2.0.CO;2), 1969.

702 French, H. M.: Surface Features of Permafrost, in: *The Periglacial Environment*, 116-152,  
703 <https://doi.org/10.1002/9781118684931.ch6>, 2007.

704 French, H. M. and Millar, S. W. S.: Permafrost at the time of the Last Glacial Maximum (LGM) in North America,  
705 *Boreas*, 43, 667-677, <https://doi.org/10.1111/bor.12036>, 2014.

706 Fritz, P., Morgan, A. V., Eicher, U., and McAndrews, J. H.: Stable isotope, fossil coleoptera and pollen stratigraphy  
707 in late quaternary sediments from Ontario and New York state, *Palaeogeography, Palaeoclimatology, Palaeoecology*,  
708 58, 183-202, [https://doi.org/10.1016/0031-0182\(87\)90059-9](https://doi.org/10.1016/0031-0182(87)90059-9), 1987.

709 Fullerton, D. S.: Preliminary correlation of post-Erie interstadial events :(16,000-10,000 radiocarbon years before  
710 present), central and eastern Great Lakes region, and Hudson, Champlain, and St. Lawrence Lowlands, United  
711 States and Canada, <https://doi.org/10.3133/pp1089>, 1980.

712 Galbraith, R. F. and Roberts, R. G.: Statistical aspects of equivalent dose and error calculation and display in OSL  
713 dating: An overview and some recommendations, *Quaternary Geochronology*, 11, 1-27,  
714 <https://doi.org/10.1016/j.quageo.2012.04.020>, 2012.

715 Gao, C.: Ice-wedge casts in Late Wisconsinan glaciofluvial deposits, southern Ontario, Canada, *Canadian Journal of*  
716 *Earth Sciences*, 42, 2117-2126, <https://doi.org/10.1139/e05-072>, 2005.

717 Gao, C.: Relict Thermal-contraction-crack Polygons and Past Permafrost South of the Late Wisconsinan Glacial  
718 Limit in the Mid-Atlantic Coastal Plain, USA, *Permafrost and Periglacial Processes*, 25, 144-149,  
719 <https://doi.org/10.1002/ppp.1803>, 2014.

720 Gill, J. L., Williams, J. W., Jackson, S. T., Donnelly, J. P., and Schellinger, G. C.: Climatic and megaherbivory  
721 controls on late-glacial vegetation dynamics: a new, high-resolution, multi-proxy record from Silver Lake, Ohio,  
722 *Quaternary Science Reviews*, 34, 66-80, <https://doi.org/10.1016/j.quascirev.2011.12.008>, 2012.

723 Glover, K. C., Lowell, T. V., Wiles, G. C., Pair, D., Applegate, P., and Hajdas, I.: Deglaciation, basin formation and  
724 post-glacial climate change from a regional network of sediment core sites in Ohio and eastern Indiana, *Quaternary*  
725 *Research*, 76, 401-410, <https://doi.org/10.1016/j.yqres.2011.06.004>, 2011.

726 Gonzales, L. M. and Grimm, E. C.: Synchronization of late-glacial vegetation changes at Crystal Lake, Illinois, USA  
727 with the North Atlantic Event Stratigraphy, *Quaternary Research*, 72, 234-245,  
728 <https://doi.org/10.1016/j.yqres.2009.05.001>, 2009.

729 Grigg, L. D., Engle, K. J., Smith, A. J., Shuman, B. N., and Mandl, M. B.: A multi-proxy reconstruction of climate  
730 during the late-Pleistocene to early Holocene transition in the northeastern, USA, *Quaternary Research*, 102,  
731 188-204, <https://doi.org/10.1017/qua.2020.127>, 2021.

732 Grootes, P. M. and Stuiver, M.: GISP2 Oxygen Isotope Data, PANGAEA [dataset],  
733 <https://doi.org/10.1594/PANGAEA.56094>, 1999.

734 Halsted, C. T., Bierman, P. R., Shakun, J. D., Davis, P. T., Corbett, L. B., Drebber, J. S., and Ridge, J. C.: A critical  
735 re-analysis of constraints on the timing and rate of Laurentide Ice Sheet recession in the northeastern United States,  
736 *Journal of Quaternary Science*, <https://doi.org/10.1002/jqs.3563>, 2023.

737 Heath, S. L., Loope, H. M., Curry, B. B., and Lowell, T. V.: Pattern of southern Laurentide Ice Sheet margin position  
738 changes during Heinrich Stadials 2 and 1, *Quaternary Science Reviews*, 201, 362-379,  
739 <https://doi.org/10.1016/j.quascirev.2018.10.019>, 2018.

740 Heiri, O., Lotter, A. F., and Lemcke, G.: Loss on ignition as a method for estimating organic and carbonate content  
741 in sediments: reproducibility and comparability of results, *Journal of Paleolimnology*, 25, 101-110,  
742 <https://doi.org/10.1023/A:1008119611481>, 2001.

743 Henriksen, M., Mangerud, J., Matiouchkov, A., Paus, A., and Svendsen, J. I.: Lake stratigraphy implies an 80 000 yr  
744 delayed melting of buried dead ice in northern Russia, *Journal of Quaternary Science*, 18, 663-679,  
745 <https://doi.org/10.1002/jqs.788>, 2003.

746 Higley, M. C., Fisher, T. G., Jol, H. M., Lepper, K., and Martin-Hayden, J. M.: Stratigraphic and chronologic  
747 analysis of the Warren Beach, northwest Ohio, USA, *Canadian Journal of Earth Sciences*, 51, 737-749,  
748 <https://doi.org/10.1139/cjes-2014-0047>, 2014.

749 Keeley, J. E. and Sandquist, D. R.: Carbon: freshwater plants, *Plant Cell & Environment*, 15,  
750 <https://doi.org/10.1111/j.1365-3040.1992.tb01653.x>, 1992.

751 Kozłowski, A. L., Bird, B. C., Lowell, T. V., Smith, C. A., Feranec, R. S., and Graham, B. L.: Minimum age of the  
752 Mapleton, Tully, and Labrador Hollow moraines indicates correlation with the Port Huron Phase in central New  
753 York State, in: *Quaternary Glaciation of the Great Lakes Region: Process, Landforms, Sediments, and Chronology*,  
754 [https://doi.org/10.1130/2018.2530\(10\)](https://doi.org/10.1130/2018.2530(10)), 2018.

755 LaFleur, R. G.: Glacial geology and stratigraphy of Western New York Nuclear Service Center and vicinity,  
756 Cattaraugus and Erie Counties, New York, Report 79-989, <https://doi.org/10.3133/ofr79989>, 1979.

757 Last, W. and Smol, J.: Tracking environmental change using lake sediments. 2. Physical and geochemical methods,  
758 <https://doi.org/10.1007/0-306-47670-3>, 2001.

759 Lewis, C. F. M. and Anderson, T. W.: A younger glacial Lake Iroquois in the Lake Ontario basin, Ontario and New  
760 York: re-examination of pollen stratigraphy and radiocarbon dating, *Canadian Journal of Earth Sciences*, 57,  
761 453-463, <https://doi.org/10.1139/cjes-2019-0076>, 2019.

762 Leydet, D. J., Carlson, A. E., Teller, J. T., Breckenridge, A., Barth, A. M., Ullman, D. J., Sinclair, G., Milne, G. A.,  
763 Cuzzone, J. K., and Caffee, M. W.: Opening of glacial Lake Agassiz's eastern outlets by the start of the Younger  
764 Dryas cold period, *Geology*, 46, 155-158, <https://doi.org/10.1130/G39501.1>, 2018.

765 Löfverström, M., Caballero, R., Nilsson, J., and Kleman, J.: Evolution of the large-scale atmospheric circulation in  
766 response to changing ice sheets over the last glacial cycle, *Climate of the Past*, 10, 1453-1471,  
767 <https://doi.org/10.5194/cp-10-1453-2014>, 2014.

768 Lusch, D. P., Stanley, K. E., Schaetzl, R. J., Kendall, A. D., Van Dam, R. L., Nielsen, A., Blumer, B. E., Hobbs, T.  
769 C., Archer, J. K., Holmstadt, J. L. F., and May, C. L.: Characterization and Mapping of Patterned Ground in the  
770 Saginaw Lowlands, Michigan: Possible Evidence for Late-Wisconsin Permafrost, *Annals of the Association of*  
771 *American Geographers*, 99, 445-466, <https://doi.org/10.1080/00045600902931629>, 2009.

772 MacClintock, P. and Apfel, E. T.: Correlation of the drifts of the Salamanca re-entrant, New York, *Bulletin of the*  
773 *Geological Society of America*, 55, 1143-1164, <https://doi.org/10.1130/GSAB-55-1143>, 1944.

774 Miller, N. G.: Late-glacial and postglacial vegetation change in southwestern New York State, University of the  
775 State of New York, State Education Dept, Albany, <https://www.biodiversitylibrary.org/bibliography/135533>, 1973.

776 Morgan, A. V.: Distribution and probable age of relict permafrost features in south-western Ontario, 4th Canadian  
777 Permafrost Conference, Ottawa, Ontario, 91-100,

778 Muller, E. H. and Calkin, P. E.: Timing of Pleistocene glacial events in New York State, *Canadian Journal of Earth*  
779 *Sciences*, 30, 1829-1845, <https://doi.org/10.1139/e93-161>, 1993.

780 Muller, E. H. and Prest, V. K.: Glacial Lakes in the Ontario Basin, in: *Quaternary Evolution of the Great Lakes*  
781 edited by: Karrow, P. F., and Calkin, P., E., Geological Society of Canada,  
782 [https://doi.org/10.1016/0033-5894\(87\)90011-1](https://doi.org/10.1016/0033-5894(87)90011-1), 1985.

783 Murray, A. S. and Wintle, A. G.: Luminescence dating of quartz using an improved single-aliquot regenerative-dose  
784 protocol, *Radiation Measurements*, 32, 57-73, [https://doi.org/10.1016/S1350-4487\(99\)00253-X](https://doi.org/10.1016/S1350-4487(99)00253-X), 2000.

785 Oana, S. and Deevey, E. S.: Carbon 13 in lake waters and its possible bearing on paleolimnology, *American Journal*  
786 *of Science*, 258-A, 253-272, 1960.

787 Olley, J. M., Caitcheon, G. G., and Roberts, R. G.: The origin of dose distributions in fluvial sediments, and the  
788 prospect of dating single grains from fluvial deposits using optically stimulated luminescence, *Radiation*  
789 *Measurements*, 30, 207-217, [https://doi.org/10.1016/S1350-4487\(99\)00040-2](https://doi.org/10.1016/S1350-4487(99)00040-2), 1999.

790 Olsson, I.: Radiometric Methods, in: *Handbook of Holocene paleoecology and paleohydrology*, edited by: Berglund,  
791 B., John Wiley & Sons, Chichester, 273-312, <https://doi.org/10.1002/gea.3340040208>, 1986.

792 Osman, M. B., Tierney, J. E., Zhu, J., Tardif, R., Hakim, G. J., King, J., and Poulsen, C. J.: Globally resolved surface  
793 temperatures since the Last Glacial Maximum, *Nature*, 599, 239-244, <https://doi.org/10.1038/s41586-021-03984-4>,  
794 2021.

795 Pearson, A., McNichol, A. P., Schneider, R. J., Von Reden, K. F., and Zheng, Y.: Microscale AMS 14C Measurement  
796 at NOSAMS, *Radiocarbon*, 40, 61-75, <https://doi.org/10.1017/S0033822200017902>, 1997.

797 Peteet, D. M., Beh, M., Orr, C., Kurdyla, D., Nichols, J., and Guilderson, T.: Delayed deglaciation or extreme Arctic  
798 conditions 21-16 cal. kyr at southeastern Laurentide Ice Sheet margin?, *Geophysical Research Letters*, 39, n/a-n/a,  
799 <https://doi.org/10.1029/2012GL051884>, 2012.

800 Porreca, C., Briner, J. P., and Kozłowski, A.: Laurentide ice sheet meltwater routing along the Iro-Mohawk River,  
801 eastern New York, USA, *Geomorphology*, 303, 155-161, <https://doi.org/10.1016/j.geomorph.2017.12.001>, 2018.

802 Ramsey, K.: Geologic map of New Castle county, Delaware: Delaware Geological Survey Geologic Map Series, 13,  
803 2005.

804 Ramsey, K.: Geologic map of Kent County, Delaware: Delaware Geological Survey Geologic Map Series, 2007.

805 Rayburn, J. A., Franzi, D. A., and Knuepfer, P. L. K.: Evidence from the Lake Champlain Valley for a later onset of  
806 the Champlain Sea and implications for late glacial meltwater routing to the North Atlantic, *Palaeogeography*,  
807 *Palaeoclimatology*, *Palaeoecology*, 246, 62-74, <https://doi.org/10.1016/j.palaeo.2006.10.027>, 2007.

808 Rayburn, J. A., Knuepfer, P. L., and Franzi, D. A.: A series of large, Late Wisconsinan meltwater floods through  
809 the Champlain and Hudson Valleys, New York State, USA, *Quaternary Science Reviews*, 24, 2410-2419,  
810 <https://doi.org/10.1016/j.quascirev.2005.02.010>, 2005.

811 Rayburn, J. A., Cronin, T. M., Franzi, D. A., Knuepfer, P. L. K., and Willard, D. A.: Timing and duration of North  
812 American glacial lake discharges and the Younger Dryas climate reversal, *Quaternary Research*, 75, 541-551,  
813 <https://doi.org/10.1016/j.yqres.2011.02.004>, 2011.

814 Reimer, P. J., Austin, W. E. N., Bard, E., Bayliss, A., Blackwell, P. G., Bronk Ramsey, C., Butzin, M., Cheng, H.,  
815 Edwards, R. L., Friedrich, M., Grootes, P. M., Guilderson, T. P., Hajdas, I., Heaton, T. J., Hogg, A. G., Hughen, K.  
816 A., Kromer, B., Manning, S. W., Muscheler, R., Palmer, J. G., Pearson, C., van der Plicht, J., Reimer, R. W.,  
817 Richards, D. A., Scott, E. M., Southon, J. R., Turney, C. S. M., Wacker, L., Adolphi, F., Büntgen, U., Capano, M.,  
818 Fahrni, S. M., Fogtmann-Schulz, A., Friedrich, R., Köhler, P., Kudsk, S., Miyake, F., Olsen, J., Reinig, F., Sakamoto,  
819 M., Sookdeo, A., and Talamo, S.: The IntCal20 Northern Hemisphere Radiocarbon Age Calibration Curve (0–55 cal  
820 kBP), *Radiocarbon*, 62, 725-757, <https://doi.org/10.1017/RDC.2020.41>, 2020.

821 Richard, P. J. H. and Occhietti, S.: 14C chronology for ice retreat and inception of Champlain Sea in the St.  
822 Lawrence Lowlands, Canada, *Quaternary Research*, 63, 353-358, <https://doi.org/10.1016/j.yqres.2005.02.003>, 2005.

823 Ridge, J. C.: The last deglaciation of the northeastern United States: a combined varve, paleomagnetic, and  
824 calibrated 14C chronology, in: *Geoarchaeology of landscapes in the glaciated northeast*, edited by: Hart, J. P., and  
825 Cremeens, D. L., *New York State Museum Bulletin*, 15-45, 2003.

826 Ridge, J. C., Balco, G., Bayless, R. L., Beck, C. C., Carter, L. B., Dean, J. L., Voytek, E. B., and Wei, J. H.: The new  
827 North American Varve Chronology: A precise record of southeastern Laurentide Ice Sheet deglaciation and climate,  
828 18.2-12.5 kyr BP, and correlations with Greenland ice core records, *American Journal of Science*, 312, 685-722,  
829 <https://doi.org/10.2475/07.2012.01>, 2012.

830 Rittenour, T. M., Cotter, J. F. P., and Arends, H. E.: Application of single-grain OSL dating to ice-proximal deposits,  
831 glacial Lake Benson, west-central Minnesota, USA, *Quaternary Geochronology*, 30, 306-313,  
832 <https://doi.org/10.1016/j.quageo.2015.02.025>, 2015.

833 Schomacker, A.: What controls dead-ice melting under different climate conditions? A discussion, *Earth-Science*  
834 *Reviews*, 90, 103-113, <https://doi.org/10.1016/j.earscirev.2008.08.003>, 2008.

835 Shah Walter, S. R., Gagnon, A. R., Roberts, M. L., McNichol, A. P., Gaylord, M. C. L., and Klein, E.: Ultra-Small  
836 Graphitization Reactors for Ultra-Microscale 14C Analysis at the National Ocean Sciences Accelerator Mass  
837 Spectrometry (NOSAMS) Facility, *Radiocarbon*, 57, 109-122, [https://doi.org/10.2458/azu\\_rc.57.18118](https://doi.org/10.2458/azu_rc.57.18118), 2015.

838 Shuman, B., Webb Iii, T., Bartlein, P., and Williams, J. W.: The anatomy of a climatic oscillation: vegetation change  
839 in eastern North America during the Younger Dryas chronozone, *Quaternary Science Reviews*, 21, 1777-1791,  
840 [https://doi.org/10.1016/S0277-3791\(02\)00030-6](https://doi.org/10.1016/S0277-3791(02)00030-6), 2002.

841 Stanford, S. D., Stone, B. D., Ridge, J. C., Witte, R. W., Pardi, R. R., and Reimer, G. E.: Chronology of Laurentide  
842 glaciation in New Jersey and the New York City area, United States, *Quaternary Research*, 1-26,  
843 <https://doi.org/10.1017/qua.2020.71>, 2020.

844 Stuiver, M. and Polach, H. A.: Discussion Reporting of 14C Data, *Radiocarbon*, 19, 355-363,  
845 <https://doi.org/10.1017/S0033822200003672>, 1977.

846 Stuiver, M. and Reimer, P. J.: Extended 14C Data Base and Revised CALIB 3.0 14C Age Calibration Program,  
847 *Radiocarbon*, 35, 215-230, <https://doi.org/10.1017/S0033822200013904>, 1993.

848 Teller, J. T.: Controls, history, outbursts, and impact of large late-Quaternary proglacial lakes in North America, in:  
849 *The Quaternary Period in the United States*, *Developments in Quaternary Sciences*, 45-61,  
850 [https://doi.org/10.1016/S1571-0866\(03\)01003-0](https://doi.org/10.1016/S1571-0866(03)01003-0), 2003.

851 Terasmae, J.: Some problems of late Wisconsin history and geochronology in southeastern Ontario, Canadian  
852 Journal of Earth Sciences, 17, 361-381, <https://doi.org/10.1139/e80-035>, 1980.

853 Tulenko, J. P., Lofverstrom, M., and Briner, J. P.: Ice sheet influence on atmospheric circulation explains the patterns  
854 of Pleistocene alpine glacier records in North America, Earth and Planetary Science Letters, 534, 116115,  
855 <https://doi.org/10.1016/j.epsl.2020.116115>, 2020.

856 US Geological Survey: FGDC Digital Cartographic Standard for Geologic Map Symbolization (PostScript  
857 Implementation), <http://pubs.usgs.gov/tm/2006/11A02/>, 2006.

858 Vogel, J. S., Southon, J. R., Nelson, D. E., and Brown, T. A.: Performance of catalytically condensed carbon for use  
859 in accelerator mass spectrometry, Nuclear Instruments and Methods in Physics Research Section B: Beam  
860 Interactions with Materials and Atoms, 5, 289-293, [https://doi.org/10.1016/0168-583X\(84\)90529-9](https://doi.org/10.1016/0168-583X(84)90529-9), 1984.

861 Wang, Y. and Wooller, M. J.: The stable isotopic (C and N) composition of modern plants and lichens from northern  
862 Iceland: with ecological and paleoenvironmental implications, Jökull, 56, 27-38, 10.33799/jokull2006.56.027, 2006.

863 Watson, B. I., Williams, J. W., Russell, J. M., Jackson, S. T., Shane, L., and Lowell, T. V.: Temperature variations in  
864 the southern Great Lakes during the last deglaciation: Comparison between pollen and GDGT proxies, Quaternary  
865 Science Reviews, 182, 78-92, <https://doi.org/10.1016/j.quascirev.2017.12.011>, 2018.

866 Wright, H. E. and Stefanova, I.: Plant trash in the basal sediments of glacial lakes, Acta Palaeobotanica, 44, 141-146,  
867 2004.

868 Yansa, C. H., II, F. A. E., Schaetzl, R. J., Kettle, J. M., and Arbogast, A. F.: Interpreting basal sediments and plant  
869 fossils in kettle lakes: insights from Silver Lake, Michigan, USA, Canadian Journal of Earth Sciences, 57, 292-305,  
870 <https://doi.org/10.1139/cjes-2018-0338>, 2020.

871 Young, R. A., Gordon, L. M., Owen, L. A., Huot, S., and Zervas, T. D.: Evidence for a late glacial advance near the  
872 beginning of the Younger Dryas in western New York State: An event postdating the record for local Laurentide ice  
873 sheet recession, Geosphere, <https://doi.org/10.1130/GES02257.1>, 2020.

874 Yu, Z.: Rapid response of forested vegetation to multiple climatic oscillations during the last deglaciation in the  
875 northeastern United States, Quaternary Research, 67, 297-303, <https://doi.org/10.1016/j.yqres.2006.08.006>, 2007.

876 Yu, Z. and Eicher, U.: Abrupt Climate Oscillations During the Last Deglaciation in Central North America, Science,  
877 282, 2235-2238, doi:10.1126/science.282.5397.2235, 1998.